

Efficient and practical Hamiltonian simulation from time-dependent product formulas

Jan Lukas Bosse^{1,2}, Andrew M. Childs^{1,3}, Charles Derby¹, Filippo Maria Gambetta¹, Ashley Montanaro^{1,2}, and Raul A. Santos¹

¹Phasecraft Ltd.

²School of Mathematics, University of Bristol

³Department of Computer Science, Institute for Advanced Computer Studies, and Joint Center for Quantum Information and Computer Science, University of Maryland

25th June 2024

Abstract

In this work we propose an approach for implementing time-evolution of a quantum system using product formulas. The quantum algorithms we develop have provably better scaling (in terms of gate complexity and circuit depth) than a naive application of well-known Trotter formulas, for systems where the evolution is determined by a Hamiltonian with different energy scales (i.e., one part is “large” and another part is “small”). Our algorithms generate a decomposition of the evolution operator into a product of simple unitaries that are directly implementable on a quantum computer. Although the theoretical scaling is suboptimal compared with state-of-the-art algorithms (e.g., quantum signal processing), the performance of the algorithms we propose is highly competitive in practice. We illustrate this via extensive numerical simulations for several models. For instance, in the strong-field regime of the 1D transverse-field Ising model, our algorithms achieve an improvement of one order of magnitude in both the system size and evolution time that can be simulated with a fixed budget of 1000 arbitrary 2-qubit gates, compared with standard Trotter formulas.

1 Introduction

Time-dynamics simulation (TDS) of quantum systems has long been considered as a natural application where quantum computers can outperform classical ones. A quantum algorithm for TDS approximates the time-evolution operator e^{-itH} by a sequence of elementary gates. The gate complexity of this decomposition is at least linear in t in general [1, 2], and several methods have been proposed that achieve (or nearly achieve) that complexity [3–6]. These methods differ in the way they implement time evolution, have different overheads, and scale differently with the desired accuracy.

Arguably the most straightforward TDS algorithm is the use of (Trotter) product formulas [7]. This approach does not use ancilla qubits [3–5], nor does it involve potentially costly operations (such as block encodings or reflections about ancillary quantum states) [6], or any classical pre-processing (such as searching for classically optimized circuits [8, 9]). Moreover, product formulas can be more efficient in practice when simulating systems with hundreds of qubits for times that scale with the size of the system [10]. This may be due to overheads that some asymptotically better algorithms incur, and to the fact that product formula methods scale better in practice than naive bounds suggest, with dependence on commutators of terms that can naturally take advantage of spatial locality [11, 12].

Product formulas split the evolution under a Hamiltonian $H = \sum_k h_k$ into a product of the form $\prod_{jk} e^{-it_{jk}h_k}$ for some times t_{jk} . This provides an efficient simulation if each elementary exponential can be implemented efficiently. Observe that the choice of the summands that compose H is not unique. A common practice when simulating lattice systems is to represent the Hamiltonian as a sum of Pauli terms $H = \sum_k \alpha_k P_k$ and choose $h_k = \alpha_k P_k$.

In this work, we introduce several algorithms that take advantage of the structure of the Hamiltonian to achieve better error scaling than standard product formulas. This approach can leverage knowledge of the gates that can be

efficiently implemented in practice on a particular quantum computer, so we call this family of algorithms Trotter Heuristic Resource Improved Formulas for Time-dynamics (THRIFT).

Starting from a Hamiltonian generating time evolution that can be implemented with a quantum circuit with error independent of the evolution time (e.g., a Hamiltonian diagonal in the computational basis, or diagonalisable with a circuit that does not scale with the evolution time), we ask, “What is the effect of adding a perturbation to the Hamiltonian in the complexity of implementing the TDS algorithm with product formulas?”. This motivates going into the interaction picture and approximating the time-ordered operator by a product of exponentials. Reference [13] explored such an interaction-picture approach, studying approximations of the time-ordered operator through a Taylor expansion of the Dyson series, instead of using product formulas. We comment on this difference below, when we compare THRIFT with previous approaches.

THRIFT generates an efficient product-formula decomposition for time evolution of a quantum system. This decomposition has provably better scaling of both gate complexity and circuit depth than a naive application of well-known product formulas, for systems where the evolution is determined by a Hamiltonian with different energy scales (i.e., in which one part is “large” and another part is “small”, with the size of the small part quantified by a parameter α). This situation is ubiquitous in effective models describing physical systems and can occur, for example, in systems with strong short-range interactions and weaker long-range interactions. Furthermore, weak (or strong) external perturbations can be used to push a system out of equilibrium and to extract its dynamical properties. Crucially, the efficiency of the algorithm depends on the characteristics of the quantum computer itself, namely, the set of gates that are easily implementable with an error independent of the circuit depth. This is particularly useful in a Noisy Intermediate-Scale Quantum (NISQ) computer, where some types of gates can be implemented more easily than other nominally similar gates. As these formulas provide better gate complexity than naive product formulas in many instances, we expect them to be useful beyond NISQ applications as well.

In Section 2 we introduce THRIFT and show that its error scales as $O(\alpha^2 t^2)$, an improvement by a factor of α compared with standard first-order product formulas. We show that k th-order THRIFT achieves error-scaling of $O(\alpha^2 t^{k+1})$, compared to $O(\alpha t^{k+1})$ for standard k th-order formulas. We also show (in Appendix A.3) that general product formulas based directly on products of the summands of the Hamiltonian cannot achieve better scaling than α^2 . To improve the α -scaling for higher-order formulas, in Sections 3.1 and 3.2 we introduce the Magnus-THRIFT and Fer-THRIFT algorithms, respectively, which achieve an effective $O(\alpha^{k+1} t^{k+1})$ error scaling, for any $k \in \mathbb{N}$.

To complement our theoretical results that show favourable asymptotic scaling of the algorithms, in Section 4 we carry out numerical experiments comparing several product formulas with THRIFT. We analyse the error as a function of the total evolution time and the scale of the small part of the Hamiltonian α for three different models: the transverse-field Ising model in one (1D) and two dimensions (2D), the 1D Heisenberg model with random fields, and the 1D Fermi-Hubbard model. For the spin models studied, the THRIFT approach generates better product formulas in terms of gate complexity (measured as the number of CNOT or arbitrary 2-qubit gates to achieve a target error) for a wide range of evolution times and α . In the case of the transverse-field Ising and Heisenberg models, surprisingly, the complexity is better even when the interaction is stronger than the transverse field. Despite the simplicity of such models, they correctly describe the relevant physics of a wide range of materials and, in the presence of frustration, they can host exotic quantum phases of matter [14–16]. In these cases, the favourable scaling is due to the possibility of implementing the elementary evolution gates with a 2-qubit gate cost that is the same as standard product formulas. For simulations of the Fermi-Hubbard model, THRIFT methods have advantageous scaling for large enough simulation time $T \gtrsim U^{-1}$ and small scale of the hopping term t_{hop}/U . This is due to the extra cost incurred in the implementation of THRIFT in this case.

Comparison with previous approaches

Reference [13] considers the time evolution of systems with different energy scales and proposes carrying out the simulation in the interaction picture through a method called *linear combination of unitaries* (LCU), achieving a gate complexity of $O(\alpha T \text{polylog}(T\alpha/\epsilon))$ for a simulation for time T with error ϵ . Although, theoretically, the LCU method has better scaling with evolution time and simulation error than product formulas, it has also been shown empirically that product-formula approaches can perform better in practice [10]. Furthermore, the LCU method uses ancilla qubits and involves implementing both an operation that coherently performs the constituent unitaries conditioned on the ancilla and a reflection about a certain ancilla state. Our approach uses no ancillas and only involves evolution according to terms of the Hamiltonian, as it directly implements the time evolution using product formulas, achieving a gate complexity of $O(\alpha T (\alpha T/\epsilon)^{1/(k-1)})$ for arbitrary fixed k .

Reference [17] uses Lieb-Robinson bounds to create a protocol for quantum simulation of lattice models that resembles the THRIFT algorithm described in Eq. (7), but where the splitting of the Hamiltonian is decided based on the support of its summands, not on the energy scales involved in the Hamiltonian. The cost of this method is nearly optimal as a function of system size as well as evolution time and approximation error. However, in practice, this strategy may perform worse than straightforward application of product formulas [11].

After completing an initial version of this work, we became aware of Ref. [18]. There, Omelyan et al. derive a set of optimised fourth-order product formulas for a Hamiltonian $H = H_A + H_B$ by adding additional sub-steps to standard Trotter formulas and numerically minimizing the error arising from commutators (see Appendix C.1.2 for details). The generalisation to Hamiltonians with an arbitrary number of terms is described in Ref. [7]. Of particular interest for the present work is an optimised formula valid in the regime $\alpha \ll 1$ of a Hamiltonian $H = H_0 + \alpha H_1$ (denominated ‘‘Omelyan’s small A ’’ in Ref. [7]). As we discuss in Section 4, for the 1D and 2D transverse-field Ising and the 1D Heisenberg models, THRIFT outperforms this optimised formula for all the values of α we consider. On the other hand, Omelyan et al.’s optimised small A formula proves to be the most efficient algorithm in the $t_{\text{hop}}/U \ll 1$ regime of the Fermi-Hubbard model. This is mainly due to the high cost of implementing the terms arising in the THRIFT decomposition of this model.

2 Motivation and main result

Consider a Hamiltonian of the form $H = H_0 + \alpha H_1$ where $\alpha \ll 1$, the norms of H_0 and H_1 are comparable, and the unitary $U_0 = e^{-itH_0}$ can be implemented exactly for arbitrary times t with an efficient quantum circuit, with complexity independent of t . We are interested in approximating the full evolution operator $U = e^{-itH}$. The first-order Trotter formula with N steps has error [7, 11]

$$\|e^{-it(H_0+\alpha H_1)} - (e^{-i\frac{t}{N}H_0}e^{-i\frac{t}{N}\alpha H_1})^N\| \leq \frac{t^2|\alpha|}{2N} \|[H_0, H_1]\|. \quad (1)$$

We can use the fact that U_0 is implementable exactly to give a simulation with lower error. Going to the interaction (also known as intermediate) picture [19], we have

$$\begin{aligned} U &= \lim_{N \rightarrow \infty} \prod_{k=1}^N e^{-i\frac{t}{N}H_0} e^{-i\frac{t}{N}\alpha H_1}, \\ &= e^{-itH_0} \lim_{N \rightarrow \infty} e^{i\frac{(N-1)t}{N}H_0} e^{-i\frac{t}{N}\alpha H_1} e^{-i\frac{(N-1)t}{N}H_0} \dots e^{-i\frac{t}{N}\alpha H_1} e^{i\frac{t}{N}H_0} e^{-i\frac{t}{N}\alpha H_1} e^{-i\frac{t}{N}H_0} e^{-i\frac{t}{N}\alpha H_1}, \\ &= e^{-itH_0} \mathcal{T} e^{-i \int_0^t \alpha H_1(\tau) d\tau}, \end{aligned} \quad (2)$$

where in the second line we have just inserted identities between each exponential of H_1 . Here, \mathcal{T} is the time-ordering operator (which moves terms with smaller times to the right) and $H_1(t) = e^{itH_0} H_1 e^{-itH_0}$. This is a better starting expression for bounding the error. Let $[\mathcal{T} e^{-i \int_0^t \alpha H_1(\tau) d\tau}]_{\text{apx}}$ denote a product formula (to be defined) for approximating $\mathcal{T} e^{-i \int_0^t \alpha H_1(\tau) d\tau}$, and let U_{apx} denote the overall approximation to U obtained by using this formula. Then we have

$$\begin{aligned} \|U - U_{\text{apx}}\| &= \|e^{-itH_0} \mathcal{T} e^{-i \int_0^t \alpha H_1(\tau) d\tau} - e^{-itH_0} [\mathcal{T} e^{-i \int_0^t \alpha H_1(\tau) d\tau}]_{\text{apx}}\| \\ &= \|\mathcal{T} e^{-i \int_0^t \alpha H_1(\tau) d\tau} - [\mathcal{T} e^{-i \int_0^t \alpha H_1(\tau) d\tau}]_{\text{apx}}\| \end{aligned} \quad (3)$$

by invariance of the operator norm under unitary transformations. Using for example the first-order generalised Trotter formula $[\mathcal{T} e^{-i \int_0^t \alpha H_1(\tau) d\tau}]_{\text{apx}} = \mathcal{T} e^{-i \int_0^t \alpha H_1^A(\tau) d\tau} \mathcal{T} e^{-i \int_0^t \alpha H_1^B(\tau) d\tau}$ [20, 21], where $H_1(\tau) = H_1^A(\tau) + H_1^B(\tau)$ is some splitting of $H_1(\tau)$, we have

$$\begin{aligned} \|U - U_{\text{apx}}\| &= \|\mathcal{T} e^{-i \int_0^t \alpha H_1(\tau) d\tau} - \mathcal{T} e^{-i \int_0^t \alpha H_1^A(\tau) d\tau} \mathcal{T} e^{-i \int_0^t \alpha H_1^B(\tau) d\tau}\|, \\ &\leq \alpha^2 \int_0^t dv \int_0^v ds \|[H_1^A(s), H_1^B(v)]\| = O(\alpha^2 t^2), \end{aligned} \quad (4)$$

assuming that $\| [H_1^A(s), H_1^B(v)] \| = O(1)$. Note that the error now scales as α^2 instead of α . For general evolution time, we can divide the evolution into N steps, giving an error

$$\begin{aligned} \|U - U_{\text{apx}}\| &= \left\| \mathcal{T} e^{-i \int_0^t \alpha H_1(\tau) d\tau} - \prod_{j=0}^{N-1} \mathcal{T} e^{-i \int_{j \frac{t}{N}}^{(j+1) \frac{t}{N}} \alpha H_1^A(\tau) d\tau} \mathcal{T} e^{-i \int_{j \frac{t}{N}}^{(j+1) \frac{t}{N}} \alpha H_1^B(\tau) d\tau} \right\| \\ &\leq \alpha^2 \sum_{j=0}^{N-1} \int_{j \frac{t}{N}}^{(j+1) \frac{t}{N}} dv \int_{j \frac{t}{N}}^v ds \| [H_1^A(s), H_1^B(v)] \| = O\left(\frac{\alpha^2 t^2}{N}\right). \end{aligned} \quad (5)$$

To turn this approach into a useful product-formula decomposition, we describe how to implement the time-ordered exponentials. This can be done using the definition of the time-ordered exponential in the other direction,

$$\mathcal{T} e^{-i \int_a^b d\tau \alpha A(\tau)} = e^{ibH_0} e^{-i(b-a)(H_0 + \alpha A)} e^{-iaH_0}, \quad (6)$$

which is valid for any Hermitian operator $A(t) = e^{iH_0 t} A e^{-iH_0 t}$. This leads to the decomposition

$$U_{\text{apx}} = e^{-itH_0} \mathcal{T} e^{-i \int_0^t \alpha H_1^A(\tau) d\tau} \mathcal{T} e^{-i \int_0^t \alpha H_1^B(\tau) d\tau} = e^{-it(H_0 + \alpha H_1^A)} e^{itH_0} e^{-it(H_0 + \alpha H_1^B)}. \quad (7)$$

This is nothing more than the usual first-order Trotter decomposition of the Hamiltonian $H = H_0 + \alpha(H_1^A + H_1^B)$ using the summands $H_0 + \alpha H_1^A$, $-H_0$, and $H_0 + \alpha H_1^B$.

The decomposition (7) has an error α times smaller than the usual first-order Trotter formula. In particular, we have the following theorem.

Theorem 1 (THRIFT decomposition). *Given a Hamiltonian $H = H_0 + \alpha H_1$ where $H_1 = \sum_{\gamma=1}^{\Gamma} H_1^{\gamma}$, the decomposition*

$$U_{\text{apx}}(t) := e^{-itH_0} \prod_{\gamma} \left(e^{itH_0} e^{-it(H_0 + \alpha H_1^{\gamma})} \right) \quad (8)$$

approximates $U(t) = e^{-itH}$ with error

$$\|U(t) - U_{\text{apx}}(t)\| \leq \alpha^2 \int_0^t dv \int_0^v ds \sum_{\gamma_1 < \gamma_2 = 1}^{\Gamma} \| [H_1^{\gamma_1}(s), H_1^{\gamma_2}(v)] \|. \quad (9)$$

For sufficiently small time, this error is $O(\alpha^2 t^2)$.

Proof. Define the approximant

$$V^{(j)}(t) := \left(\prod_{k=1}^j \mathcal{T} e^{-i \int_0^t H_1^k(s) ds} \right) \mathcal{T} e^{-i \int_0^t \sum_{k=j+1}^{\Gamma} H_1^k(s) ds}. \quad (10)$$

Here $V^{(0)}(t) = \mathcal{T} e^{-i \int_0^t H_1(s) ds}$ corresponds to the evolution under the full Hamiltonian $H_1(t)$, while $V^{(\Gamma-1)}(t) = e^{itH_0} U_{\text{apx}}(t)$, where $U_{\text{apx}}(t)$ is defined in Eq. (8). This follows from repeated use of Eq. (6). Using the invariance of the operator norm and Eq. (4), it follows that

$$\|V^{(j)}(t) - V^{(j+1)}(t)\| \leq \alpha^2 \int_0^t dv \int_0^v ds \sum_{k=j+2}^{\Gamma} \| [H_1^{j+1}(s), H_1^k(v)] \|. \quad (11)$$

We use Eq. (11) to bound the error by applying the triangle inequality on the identity $V^{(0)} - V^{(\Gamma-1)} = \sum_{j=0}^{\Gamma-2} (V^{(j)} - V^{(j+1)})$ and noting that $\|V^{(0)}(t) - V^{(\Gamma-1)}(t)\| = \|U(t) - U_{\text{apx}}(t)\|$, which leads finally to Eq. (9) as claimed. \square

For α small the error of this approximation scales better than a normal Trotter approximation.

The THRIFT decomposition in Theorem 1 corresponds to a first-order Trotter formula, and can be used as a seed for higher-order approximations using standard techniques [1, 12, 22, 23]. More formally, we have the following procedure to turn a product formula into a THRIFT formula with $O(\alpha^2)$ error scaling.

Proposition 2 (Higher-order THRIFT). *Given a second-order product formula $\mathcal{S}_2(t)$ and a set of parameters $\{u_j\}_{j=1}^m$ such that*

$$\mathcal{S}_k(t) = \prod_{j=1}^m \mathcal{S}_2(u_j t) \quad (12)$$

is a k th-order product formula, the product

$$\mathcal{S}_k(t) = \prod_{j=1}^m U_{\text{apx}}\left(\frac{u_j}{2}t\right) U_{\text{apx}}^\dagger\left(-\frac{u_j}{2}t\right), \quad (13)$$

with $U_{\text{apx}}(t)$ specified by Eq. (8), approximates e^{-itH} with error $O(t^{k+1}\alpha^2)$.

Proof. $U_{\text{apx}}(t)$ is simply a first-order product formula with the unusual splitting

$$H = (H_0 + \alpha H_1^\Gamma) - H_0 + \dots + (H_0 + \alpha H_1^\Gamma). \quad (14)$$

It follows trivially that Eq. (13) is a k th-order product formula. To prove the $O(\alpha^2)$ error scaling, we write

$$\mathcal{S}_k(t) = e^{-i\sum_j u_j t H_0} \prod_{j=1}^m \left(\prod_{\gamma=1}^{\Gamma} \mathcal{T} e^{-i \int_{\frac{u_j}{2}t}^{(u_j+u_j)t} \alpha H_1^\Gamma(\tau) d\tau} \right) \left(\prod_{\gamma=\Gamma}^1 \mathcal{T} e^{-i \int_{\frac{u_j}{2}t}^{(u_j+\frac{u_j}{2})t} \alpha H_1^\Gamma(\tau) d\tau} \right) \quad (15)$$

with $a_{m-k} = \sum_{r=0}^{k-1} u_{m-r}$ and $a_m = 0$. This expression follows by applying Eq. (6) to Eq. (13). A valid product formula satisfies $\sum_{j=1}^m u_j = 1$, so the claim follows by Theorem 10 of Appendix A.3. \square

3 Beyond quadratic scaling

The procedure developed in Proposition 2 improves the $O(t)$ error scaling, but leaves the $O(\alpha^2)$ error scaling unchanged. In fact, in Appendix A.3 we prove that no formula that approximates the evolution by a product of time-ordered evolutions according to terms of the Hamiltonian can achieve better scaling in α than THRIFT, regardless of how the Hamiltonian is decomposed. However, in this section we show how to achieve better scaling using two alternative approaches.

Motivated by Eq. (2), we look for approximations of the time-ordered operator that have better error scaling in the small parameter α . First, we consider the Magnus expansion [24], which approximates the time-ordered exponential as the standard exponential of a time-dependent operator Ω . Second, we consider directly approximating the time-ordered exponential as a product of exponentials [25]. We show that these approaches achieve error scaling $O(t^k \alpha^k)$ for any positive integer k . We also present two algorithms to implement these approximations in practice.

3.1 Magnus-THRIFT

Writing

$$\mathcal{T} e^{-i\alpha \int_0^t H(s) ds} =: e^{\Omega(\alpha, t)} \quad (16)$$

for some time-dependent operator $\Omega(\alpha, t)$, it is easy to show that $\frac{d e^{\Omega(t)}}{dt} e^{-\Omega(t)} = -i\alpha H_1(t)$. Magnus [24] used this to find an equation for Ω by employing the inverse of the derivative of the exponential map, i.e.,

$$\frac{d e^{\Omega(t)}}{dt} e^{-\Omega(t)} = \frac{e^{\text{ad}_\Omega} - 1}{\text{ad}_\Omega} \frac{d\Omega}{dt} \rightarrow \frac{d\Omega}{dt} = \frac{\text{ad}_\Omega}{e^{\text{ad}_\Omega} - 1} (-i\alpha H_1) = \sum_{k=0}^{\infty} \frac{b_k}{k!} \text{ad}_\Omega^k (-i\alpha H_1), \quad (17)$$

where $\text{ad}_\Omega(\cdot) := [\Omega, \cdot]$ and $\text{ad}_\Omega^j(\cdot) := \text{ad}_\Omega^{j-1}([\Omega, \cdot])$. The coefficients b_j are Bernoulli numbers, defined through $\frac{x}{e^x - 1} = \sum_{j=0}^{\infty} \frac{b_j}{j!} x^j$. The equation for Ω can now be solved through Picard iteration [24, 26]. Defining α -independent

coefficients $\tilde{\Omega}_j(t)$ so that $e^{\Omega(\alpha,t)} = \exp\left(\sum_{j=1}^{\infty} \alpha^j \tilde{\Omega}_j(t)\right)$, and using this expression in Eq. (17), produces the recurrence [27]

$$\frac{d}{dt} \tilde{\Omega}_n(t) = \sum_{k=1}^{n-1} \frac{b_k}{k!} \sum_{\substack{j_1+j_2+\dots+j_k=n-1 \\ j_1, j_2, \dots, j_k \geq 1}} [\tilde{\Omega}_{j_1}(t), [\tilde{\Omega}_{j_2}(t), \dots [\tilde{\Omega}_{j_k}(t), -iH_1(t)] \dots]]. \quad (18)$$

The series for Ω converges for sufficiently small time t [28, 29] (see also Theorem 18). Using these results, we can state the following lemma bounding the terms of the Magnus expansion.

Lemma 3. For $l \geq 1$, $\|\tilde{\Omega}_l(t)\| \leq \frac{1}{2} x_l (2 \int_0^t \|H_1(s)\| ds)^l$, where x_l is the coefficient of s^l in the expansion of $G^{-1}(s) = \sum_{m=1}^{\infty} x_m s^m$, the inverse function of $G(s) = \int_0^s (2 + \frac{x}{2}(1 - \cot(x/2)))^{-1} dx$.

This lemma is mentioned in [26]. We include a proof for completeness in Appendix B. Armed with Lemma 3, we can now easily prove the following approximation theorem.

Theorem 4 (Magnus-THRIFT decomposition). Consider a Hamiltonian $H = H_0 + \alpha H_1$. Let $H_1(t) := e^{itH_0} H_1 e^{-itH_0}$. Defining $\Omega^{[k]} := \sum_{j=1}^k \Omega_j(\alpha, t)$, the operation

$$U_M(t) := e^{-itH_0} \exp\left(\Omega^{[k]}(\alpha, t)\right) = e^{-itH_0} \exp\left(\sum_{j=1}^k \alpha^j \tilde{\Omega}_j(t)\right) \quad (19)$$

approximates $U(t) = e^{-itH}$ with error $O((t\alpha)^{k+1})$ for small times t .

Proof. As $e^{-it(H_0 + \alpha H_1)} = e^{-itH_0} \mathcal{T} e^{-i\alpha \int_0^t H_1(s) ds}$, it suffices to approximate the time-ordered evolution $\mathcal{U}(\alpha, t) := \mathcal{T} e^{-i\alpha \int_0^t H_1(s) ds}$. Introducing the Taylor remainder of a function $h(\alpha)$ as $R_k(h(\alpha)) := \sum_{n=k+1}^{\infty} \frac{\alpha^n}{n!} h^{(n)}(0)$, it follows that for $\Omega(\alpha, t) = \sum_{j=1}^{\infty} \alpha^j \tilde{\Omega}_j(t)$,

$$\begin{aligned} \|R_k(\Omega(\alpha, t))\| &\leq \sum_{n=k+1}^{\infty} \alpha^n \|\tilde{\Omega}_n(t)\| \quad \text{using the triangle inequality and the definition of the remainder} \\ &\leq \frac{1}{2} \sum_{n=k+1}^{\infty} \frac{\alpha^n}{n!} \frac{d^n}{dz^n} (G^{-1}(0)) \left(2 \int_0^t \|H_1(x)\| dx\right)^n \quad \text{applying Lemma 3 termwise} \\ &= R_k\left(\frac{1}{2} G^{-1}\left(2\alpha \int_0^t \|H_1(s)\| ds\right)\right) \quad \text{using the definition of the remainder.} \end{aligned} \quad (20)$$

The remainder provides a bound on the difference between $\mathcal{U}(\alpha, t) = e^{\Omega(\alpha,t)} = e^{(\Omega^{[k]}(\alpha,t) + R_k(\Omega(\alpha,t)))}$ and $e^{\Omega^{[k]}(\alpha,t)}$ by means of the integral representation of the error

$$F := e^{\Omega(\alpha,t)} e^{-\Omega^{[k]}(\alpha,t)} - 1 = \int_0^s ds e^{s(\Omega^{[k]}(\alpha,t) + R_k(\alpha,t))} R_k(\alpha, t) e^{-s\Omega^{[k]}(\alpha,t)}. \quad (21)$$

Using Eq. (20), we have $\|\mathcal{U}(\alpha, t) - e^{\Omega^{[k]}(\alpha,t)}\| \leq R_k(\frac{1}{2} G^{-1}(\alpha t \|H_1\|))$. This implies that the error scales as $O((\alpha t)^{k+1})$. \square

Note that the above proof extends trivially to an arbitrary time-dependent $H_1(t)$.

Magnus-THRIFT Algorithm

We now describe a method for approximating the dynamics of the Hamiltonian $H = H_0 + \alpha H_1$ for time T using the Magnus expansion. The approach is as follows:

1. Write the evolution operator $U(T) = e^{-iT(H_0 + \alpha H_1)}$ in the interaction picture, with H_0 as the dominant part:

$$U(T) = e^{-iT H_0} \mathcal{T} e^{-i \int_0^T \alpha H_1(t) dt}. \quad (22)$$

2. Slice the time T into N intervals:

$$\mathcal{T}e^{-i\int_0^T \alpha H_1(t)} = \prod_{k=0}^{N-1} \mathcal{T}e^{-i\int_k \frac{T}{N} \alpha H_1(t)}. \quad (23)$$

3. Approximate the time-ordered exponential of a slice using its Magnus expansion up to order $O((\frac{T}{N}\alpha)^p)$. Note that here we use the Magnus expansion with an initial time $t_0 \neq 0$. We write the Magnus approximation of order p with an arbitrary initial time t as $\Omega(\alpha, \delta t; t)$, such that

$$\mathcal{T}e^{-i\int_t^{t+\delta t} \alpha H_1(t)} = \exp\left(\Omega^{[p]}(\alpha, \delta t; t)\right) + O((\delta t \alpha)^{p+1}). \quad (24)$$

4. Approximate the exponential $\exp(\Omega^{[p]}(\alpha, \delta t; t))$ obtained from the Magnus expansion using a p th-order product formula S_p :

$$\exp\left(\Omega^{[p]}(\alpha, \delta t; t)\right) = S_p(t, \delta t) + O((\delta t \alpha)^{p+1}). \quad (25)$$

This procedure leads to the decomposition

$$U(T) = e^{-iTH_0} \prod_{k=1}^N S_p\left(\left(k-1\right)\frac{T}{N}, \frac{T}{N}\right) + O\left(N\left(\frac{T\alpha}{N}\right)^{p+1}\right). \quad (26)$$

As an example, consider the expansion of

$$e^{\Omega^{[2]}(\alpha, t; \delta t)} = e^{-i\alpha\delta t\left(\frac{1}{\delta t}\int_t^{t+\delta t} d\tau H(\tau) - \frac{i\alpha}{2\delta t}\int_t^{t+\delta t} dt_1 \int_t^{t_1} dt_2 [H(t_1), H(t_2)]\right)}. \quad (27)$$

Expanding the time-dependent Hamiltonian as a sum of time-independent operators O_q and functions of time $\alpha_q(t)$ as $H(t) = \sum_{q=1}^Q \alpha_q(t)O_q$, we find

$$\Omega^{[2]}(t, \delta t) = -i\alpha\delta t\left(\sum_q A_q(t, \delta t)O_q + \sum_{q>p} B_{qp}(t, \delta t)[O_q, O_p]\right) \quad (28)$$

where

$$A_q(t, \delta t) = \frac{1}{\delta t} \int_t^{t+\delta t} d\tau \alpha_q(\tau), \quad (29)$$

$$B_{qp}(t, \delta t) = -\frac{i\alpha}{4\delta t} \int_t^{t+\delta t} \int_t^{t+\delta t} dt_1 dt_2 \alpha_q(t_1) \alpha_p(t_2) \text{sign}(t_1 - t_2), \quad (30)$$

which can be computed classically. Thus we can approximate $e^{\Omega^{[2]}(\alpha, t; \delta t)}$ using a second-order product formula as

$$\begin{aligned} e^{\Omega^{[2]}(\alpha, t; \delta t)} &= e^{-i\epsilon\delta t\left(\frac{1}{\delta t}\int_t^{t+\delta t} d\tau H(\tau) - \frac{i\epsilon}{2\delta t}\int_t^{t+\delta t} dt_1 \int_t^{t_1} dt_2 [H(t_1), H(t_2)]\right)} \\ &= e^{-i\epsilon\delta t\left(\sum_q A_q(t, \delta t)O_q + \sum_{q>p} B_{qp}(t, \delta t)[O_q, O_p]\right)} \\ &= e^{-i\frac{\epsilon\delta t}{2}\sum_q A_q(t, \delta t)O_q} e^{-i\epsilon\delta t\sum_{q>p} B_{qp}(t, \delta t)[O_q, O_p]} e^{-i\frac{\epsilon\delta t}{2}\sum_q A_q(t, \delta t)O_q} + O(\alpha^3\delta t^3). \end{aligned} \quad (31)$$

If necessary, each of the products can be decomposed further using a second-order product formula to keep the error at most $O(\alpha^3\delta t^3)$.

Note that in any application of these formulas, some care has to be taken when expanding functions of time, to avoid losing the favourable scaling with α . As the error scales with both α and t , in any expansion the scaling with both of them should be considered.

In principle it should be possible to analyse the commutator scaling of the product formula appearing in Eq. (26), generalizing [12]. We leave this as a topic for future work.

3.2 Fer-THRIFT

We can bypass approximating the Magnus term $e^{\Omega^{[j]}(\alpha, t; \delta t)}$ in Eq. (19) by directly looking for an approximation of the time-ordered operator as a product of exponentials. This approach generates the following decomposition.

As before, the starting point is an approximation of the time-ordered operator in the interaction picture. For this approximation, Fer [25] postulated the form

$$\mathcal{T} e^{-i \int_0^t A(s) ds} = e^{-i \int_0^t A(s) ds} V(t). \quad (32)$$

This implies the equation

$$\frac{d}{dt} V = \left[-i e^{i \int_0^t A(s) ds} A(t) e^{-i \int_0^t A(s) ds} - e^{i \int_0^t A(s) ds} \frac{d}{dt} e^{-i \int_0^t A(s) ds} \right] V =: -i A_1(t) V, \quad (33)$$

which can be formally solved as $V = \mathcal{T} e^{-i \int_0^t A_1(s) ds}$. Repeating this procedure k times gives

$$\mathcal{T} e^{-i \int_0^t A(s) ds} = \prod_{j=0}^{k-1} e^{-i \int_0^t A_j(s) ds} V_k, \quad (34)$$

where $A_0 := A$ and

$$\begin{aligned} A_j(t) &= e^{i \int_0^t A_{j-1}(s) ds} A_{j-1}(t) e^{-i \int_0^t A_{j-1}(s) ds} - i e^{i \int_0^t A_{j-1}(s) ds} \frac{d}{dt} e^{-i \int_0^t A_{j-1}(s) ds} \\ &= \sum_{m=1}^{\infty} (-1)^m \frac{m}{(m+1)!} \text{ad}_{-i \int_0^t A_{j-1}(s) ds}^m (A_{j-1}(t)). \end{aligned} \quad (35)$$

Setting $V_k = 1$ truncates this product, giving an approximation of order $O(t^{2^{k+1}-1})$ [30].

This analysis can be modified slightly to determine how the error depends on a scaling factor α by making the substitution $A_0 \rightarrow \alpha A_0$. For the following we absorb the factor of $-i$ into A_0 as it does not change the analysis.

Lemma 5. *Let $A_0(t)$ be an operator-valued function that is analytic in t over the reals. For a real scaling factor α , define $\alpha A_k(t)$ recursively as*

$$\alpha A_{k+1}(t) = \sum_{m=1}^{\infty} (-1)^m \frac{m}{(m+1)!} \text{ad}_{\int_0^t \alpha A_k(s) ds}^m [\alpha A_k(t)]. \quad (36)$$

If $\alpha A_k(t) = O(\alpha^q t^p)$ then $\alpha A_{k+1}(t) = O(\alpha^{2q} t^{2p+2})$.

Proof. The proof is largely similar to the proof of Lemma 2 of [30], differing in the fact that it also tracks the scaling variable α . For notational compactness, let $\alpha B_k(t) = \int_0^t \alpha A_k(s) ds$.

By Lemma 1 of [30], αA_k is analytic in t over the reals for all k . As $A_k(t)$ has no dependence on α , they are also analytic over all α . We may then write

$$\begin{aligned} \alpha A_k(t) &= \sum_{i=0}^{2p+1} \frac{1}{i!} \alpha A_k^{(i)}(0) t^i + \alpha^q t^{2p+2} E_A(\alpha, t), \\ \alpha B_k(t) &= \sum_{i=1}^{2p+1} \frac{1}{i!} \alpha A_k^{(i-1)}(0) t^i + \alpha^q t^{2p+2} E_B(\alpha, t), \end{aligned} \quad (37)$$

where the superscripts of A_k denote derivatives with respect to t .

By the bilinearity of the commutator, we have

$$[\alpha B_k(t), \alpha A_k(t)] = \sum_{i=1}^{\infty} \sum_{j=0}^{\infty} \frac{1}{i! j!} [\alpha A_k^{(i-1)}(0), \alpha A_k^{(j)}(0)] t^{i+j} + \alpha^{2q} t^{2p+2} E_1(\alpha, t) \quad (38)$$

where we have used the fact that $\alpha A_k^{(i)}(0) \in O(\alpha^q)$. Reordering the summation gives

$$[\alpha B_k(t), \alpha A_k(t)] = \sum_{i=1}^{\infty} \frac{1}{i!} \left[\sum_{j=0}^j \binom{i}{j} [\alpha A_k^{(i-j-1)}(0), \alpha A_k^{(j)}(0)] \right] t^i + \alpha^{2q} t^{2p+2} E_2(\alpha, t). \quad (39)$$

As $\alpha A_k(t) = O(t^p)$, $\alpha A_k^{(j)}(0) = 0$ for $0 \leq j \leq p-1$, so for $i \leq 2p$,

$$\sum_{j=0}^j \binom{i}{j} [\alpha A_k^{(i-j-1)}(0), \alpha A_k^{(j)}(0)] = 0 \quad (40)$$

and

$$\sum_{j=0}^{2p+1} \binom{2p+1}{j} [\alpha A_k^{(2p-j)}(0), \alpha A_k^{(j)}(0)] = \binom{2p+1}{p} [\alpha A_k^{(p)}(0), \alpha A_k^{(p)}(0)] = 0. \quad (41)$$

Therefore $[\alpha B_k(t), \alpha A_k(t)] = O(\alpha^{2q} t^{2p+2})$. For the nested commutators we have

$$\text{ad}_{\alpha B_k(t)}^m [\alpha A_k(t)] = O(\alpha^{mk} t^{m(p+1)}) \quad (42)$$

because $\alpha B_k(t) = O(\alpha^q t^{p+1})$, so $\alpha A_{k+1}(t) = O(\alpha^{2q} t^{2p+2})$ as claimed. \square

Theorem 6. *Let*

$$\begin{aligned} U(t) &= \mathcal{T} e^{\int_0^t \alpha A_0(s) ds}, \\ U_F(t) &= \prod_{j=0}^{k-1} e^{\int_0^t \alpha A_j(s) ds}, \end{aligned} \quad (43)$$

with A_j defined as in Lemma 5. Then

$$\|U_F(t) - U(t)\| = O(\alpha^{2^k} t^{2^{k+1}-1}). \quad (44)$$

Proof. The proof of Theorem 3 of [30] shows that

$$U_F(t) - U(t) = - \int_0^t U(t-\tau) U_F(\tau) \alpha A_k(\tau) d\tau. \quad (45)$$

The bound follows since $U(t), U_F(t) = O(1)$ and $\alpha A_k(t) = O(\alpha^{2^k} t^{2^{k+1}-2})$. \square

For an approximation of the total evolution in the interaction picture, we have the following.

Corollary 7 (Fer-THRIFT decomposition). *Consider a Hamiltonian $H = H_0 + \alpha H_1$, and let $H_1(t) = e^{itH_0} H_1 e^{-itH_0}$. Define*

$$U_F(t) = e^{-itH_0} \prod_{j=0}^{k-1} e^{-i \int_0^t A_j(s) ds}, \quad (46)$$

where $A_j(t)$ is defined recursively from Eq. (35) with $A_0(t) := \alpha H_1(t)$. Then $U_F(t)$ approximates $U(t) = e^{-itH}$ up to $O(\alpha^{2^k} t^{2^{k+1}-1})$ for small times t .

Note that the surprising scaling of this approach with t and α is due to the assumption that the unitaries $e^{-i \int_0^t A_j(s) ds}$ can be implemented exactly. In any actual implementation, these unitaries have to be approximated up to the target error, thus recovering in practice the same scaling as Magnus-THRIFT. This is exemplified in the following algorithm.

Fer-THRIFT Algorithm

To approximate the time evolution generated by the Hamiltonian $H = H_0 + \alpha H_1$ for time T with precision $O(N(T\alpha/N)^{p+1})$, we perform the following:

1. Write the evolution operator $U(T) = e^{-iT(H_0 + \alpha H_1)}$ in the interaction picture, with H_0 as the dominant part, i.e.,

$$U(T) = e^{-iTH_0} \mathcal{T} e^{-i \int_0^T \alpha H_1(t)}. \quad (47)$$

2. Slice the time T into N intervals:

$$\mathcal{T} e^{-i \int_0^T \alpha H_1(t)} = \prod_{k=1}^N \mathcal{T} e^{-i \int_{(k-1)\frac{T}{N}}^{\frac{kT}{N}} \alpha H_1(t)}. \quad (48)$$

3. Approximate the time-ordered exponential of a slice using its Fer expansion up to order $O((\frac{T}{N}\alpha)^p)$:

$$\mathcal{T} e^{-i \int_t^{t+\delta t} \alpha H_1(t)} = \prod_{j=0}^{\log(p)} \exp\left(-i \int_t^{t+\delta t} A_j(s) ds\right) + O((\delta t \alpha)^{p+1}). \quad (49)$$

4. Approximate each exponential in the product using a p th-order formula:

$$\exp\left(-i \int_t^{t+\delta t} A_j(s) ds\right) = S_p^j(t, \delta t) + O((\delta t \alpha)^{p+1}). \quad (50)$$

This procedure leads to the decomposition

$$U(T) = e^{-iTH_0} \prod_{k=1}^N \prod_{j=0}^{\log(p)} S_p^j\left((k-1)\frac{T}{N}, \frac{T}{N}\right) + O\left(N\left(\frac{T\alpha}{N}\right)^{p+1}\right). \quad (51)$$

Note that for the error in the resulting simulation to have the stated scaling, the unitary e^{-iTH_0} must be implemented with error at most $O((T\alpha)^{p+1})$.

4 Numerical results

The asymptotics derived in [Theorems 1](#) and [4](#) show that for α small enough, THRIFT methods will outperform Trotter methods, and for even smaller α , Magnus-THRIFT will eventually outperform THRIFT. Similarly, higher-order methods will outperform lower-order methods for small enough time steps. To ascertain that THRIFT and Magnus-THRIFT methods give an advantage at relevant values of α and T , we performed extensive simulations of different models, namely the transverse-field Ising model in one and two dimensions ([Section 4.1](#)), the Heisenberg model with random local fields in one dimension ([Section 4.2](#)), and the Fermi-Hubbard model in one dimension ([Section 4.3](#)).

We compare the ordinary first- and second-order product formulas [[1](#), [12](#)] (here dubbed ‘‘Trotter 1’’ and ‘‘Trotter 2’’), the fourth-order formula due to Suzuki [[22](#)] (here dubbed ‘‘Trotter 4’’ for conciseness), a numerically optimised eighth-order product formula due to Morales et al. [[23](#)] (‘‘optimised Trotter 8’’) based on an ansatz of Yoshida [[31](#)], and a fourth-order formula optimised for Hamiltonians containing a small perturbation derived in Ref. [[18](#)] (here dubbed ‘‘opt. small A 4’’ to indicate its error scaling with T). For each of these product formulas, we also construct the corresponding THRIFT circuit (dubbed ‘‘THRIFT 1’’ through ‘‘THRIFT 4’’ and ‘‘optimised THRIFT 8’’) as described in [Theorem 1](#) and [Proposition 2](#). For the transverse-field Ising model, we also implement the Magnus-THRIFT decompositions described in [Theorem 4](#) with the first- and second-order Magnus expansion.

In the numerical implementation of THRIFT 1 through 8, we use the approximant

$$(U_{\text{apx}}(T/N))^N = \left(e^{-i\frac{T}{N}H_0} \prod_{\gamma} \left(e^{i\frac{T}{N}H_0} e^{-i\frac{T}{N}(H_0 + \alpha H_1^{\gamma})} \right)^N \right)^N,$$

Algorithm	2-qubit gate depth	CNOT depth	# steps in Fig. 1
Trotter 1	$2N$	$4N$	15
Trotter 2	$2N + 1$	$4N + 2$	15
Trotter 4	$10N + 1$	$20N + 2$	3
optimised Trotter 8	$30N + 1$	$60N + 2$	1
THRIFT 1	$2N$	$4N + 2$	15
THRIFT 2	$2N + 1$	$4N + 2$	15
THRIFT 4	$10N + 1$	$20N + 2$	3
optimised THRIFT 8	$30N + 1$	$60N + 2$	1
Magnus-THRIFT 1	$2N$	$4N$	15
Magnus-THRIFT 2	$12N + 3$	$36N + 9$	2
optimised small A 4	$12N$	$24N$	2

Table 1: Circuit depth comparison of the different TDS algorithms investigated and shown in Fig. 1 for the 1D transverse-field Ising model. The first column shows the 2-qubit depth of the circuit corresponding to N Trotter steps in terms of arbitrary 2-qubit gates. The second column shows the corresponding cost in terms of CNOT gates. Finally, the third column gives the number of Trotter steps used in Fig. 1, which correspond to a fixed budget of arbitrary 2-qubit gates of 31.

obtained by first breaking up the total time T into small steps T/N and then approximating each unitary evolution over a small step by Eq. (8). For a total time-independent Hamiltonian H , this is equivalent to splitting the time-ordered exponential over the full evolution time into a product of unitary evolutions with a small time step T/N , as described in Eqs. (22) and (23).

Note that Fer-THRIFT 1 and Magnus-THRIFT 1 coincide. As we found that Magnus-THRIFT 2 was not generally competitive with the other approaches for the systems we analysed, we did not implement Fer-THRIFT 2 as it has essentially the same cost as Magnus-THRIFT 2.

4.1 1D and 2D transverse-field Ising model with weak coupling

The first model we use for numerical tests and algorithm comparison is the transverse-field Ising model with weak interaction in one and two dimensions. In the 1D case, the model is integrable and can be mapped to a free-fermion model that can be simulated in polynomial time and space using the method described in [32, 33]. This enables us to simulate chains of length up to $L = 100$ using the fermionic linear optics simulation tools from [34]. While the equivalence to free fermions makes this model a less interesting target for quantum simulation, we expect that the simulation costs may be indicative of costs for some other 1D models that are not necessarily classically easy. Indeed, we see evidence of this in the case of the Heisenberg model, as shown in Section 4.2. In 2D, we are restricted to relatively small system sizes using full state vector simulations.

The Hamiltonian of the transverse-field Ising model is

$$H_{\text{TFIM}} = h \sum_j Z_j + J \sum_{\langle i,j \rangle} X_i X_j, \quad (52)$$

where X_i and Z_i are the spin-1/2 operators in the x and z directions, respectively. For the purpose of studying THRIFT-based algorithms, we fix the field strength to $h = 1$, let the interaction strength $\alpha := J$ be the small parameter, and measure time T in units of h^{-1} . Since the transverse-field part, $H_0 = \sum_j Z_j$, only consists of one-qubit terms, this has the advantage that the interaction-picture Hamiltonian $H_1(t)$ has the same locality as the original $H_1 = J \sum_{\langle i,j \rangle} X_i X_j$, and THRIFT circuits have the same 2-qubit gate depth as the corresponding Trotter circuits. We also note that, because $e^{-itJX_i X_j}$ and $e^{-it(JX_i X_j + h(Z_i + Z_j))}$ can be implemented with the same number of CNOT gates—namely two—the same holds for CNOT gate depth. The 2-qubit gate depths of one TDS step for all algorithms considered are shown in Table 1. The explicit formulas for the approximants used for the THRIFT simulations of the transverse-field Ising model are discussed in Appendix C.2.1.

In Fig. 1 we show which of the different Trotter, THRIFT, or Magnus-THRIFT algorithms performs best at a given T and α for a wide range of these two quantities for the 1D transverse-field Ising model (top) and 2D transverse-field Ising model (bottom). The results broadly agree with what we expect from Theorems 1 and 4 and Proposition 2:

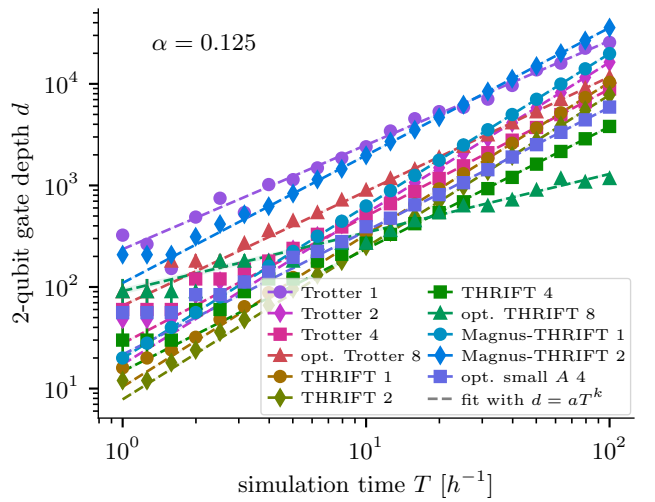
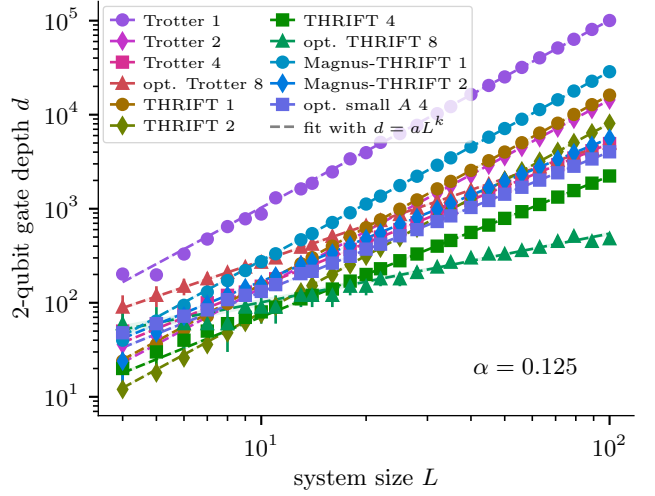
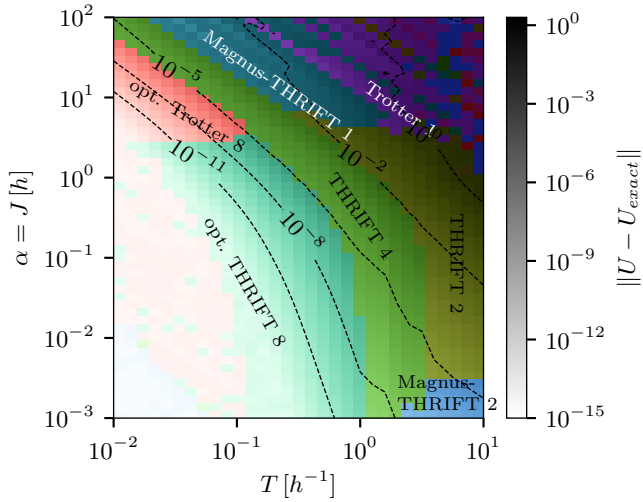
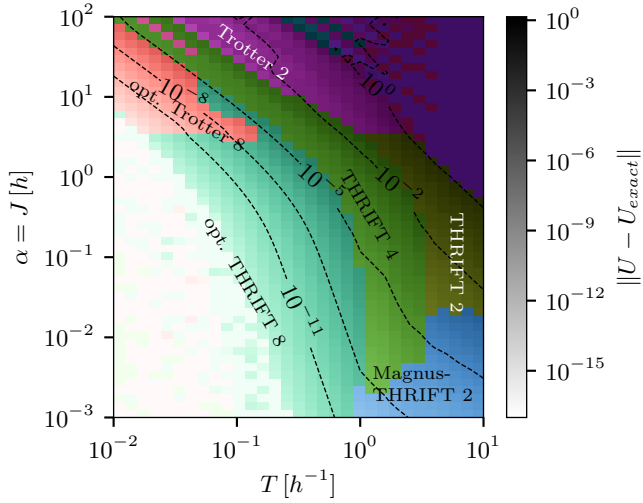


Figure 1: (top) Landscape of the best TDS algorithm, as measured by the worst-case error $\|U - U_{\text{exact}}\|$, as a function of the relative field strength $\alpha = J/h$ and evolution time T at identical circuit depth for a 1×16 Ising chain with transverse field. The circuit depth was fixed to 1 step of Magnus-THRIFT 2 evolution. For the other algorithms, the number of steps is chosen to match the 2-qubit depth as closely as possible according to the 2-qubit depths shown in Tables 1 and 2. The colour of each point represents the algorithm that achieves the lowest error at those values of J and T , while the brightness indicates the magnitude of the error. (bottom) Same for a 3×3 transverse-field Ising model. Note that in the top right corner of both panels, $\|U - U_{\text{exact}}\|$ is of order 1, so this region is not of particular interest

Figure 2: (top) 2-qubit gate depth to achieve $\|U - U_{\text{exact}}\| \leq 0.01$ for the different TDS algorithms for a field strength of $J = 1/8$ and evolution time $T = L$, for a $1 \times L$ Ising chain with transverse field. The depths follow a power law of the form $d = aL^k$ whose parameters a and k we determine via a least-squares fit and report, also for different values of α , in Fig. 10. (bottom) Similar simulation for a 3×3 transverse-field Ising model. Because the 2D transverse-field Ising model is not integrable and hence large system sizes are not classically simulable, we fix the system size to 3×3 and only scale the evolution time T . Error bars (mostly barely visible) are ± 1 , i.e., the minimal possible depth resolution.

Algorithm	2-qubit gate depth	CNOT depth	# steps in Fig. 1
Trotter 1	$4N$	$8N$	26
Trotter 2	$6N + 1$	$12N + 2$	17
Trotter 4	$30N + 1$	$60N + 2$	3
optimised Trotter 8	$90N + 1$	$180N + 2$	1
THRIFT 1	$4N$	$8N + 2$	26
THRIFT 2	$6N + 1$	$12N + 2$	17
THRIFT 4	$30N + 1$	$60N + 2$	3
optimised THRIFT 8	$90N + 1$	$180N + 2$	1
Magnus-THRIFT 1	$4N$	$8N$	26
Magnus-THRIFT 2	$102N + 3$	$306N + 9$	1
optimised small A 4	$28N$	$56N$	3

Table 2: Circuit depth comparison of the different TDS algorithms investigated and shown in Fig. 1 for the 2D transverse-field Ising model. The first column shows the 2-qubit depth of the circuit corresponding to N Trotter steps in terms of arbitrary 2-qubit gates. The second column shows the corresponding cost in terms of CNOT gates. Finally, the third column gives the number of Trotter steps used in Fig. 1, which correspond to a fixed budget of arbitrary 2-qubit gates of 105.

as T decreases, higher-order formulas become advantageous over lower orders, and for smaller α , THRIFT methods are advantageous over Trotter methods. Interestingly, this crossover happens for a relatively large $\alpha \approx 3$ for the transverse-field Ising model. First-order methods are never advantageous for the 1D transverse-field Ising model, because for Hamiltonians that can be split into only two exactly implementable parts for Trotterisation, second-order methods have the same amortised depth per step as first-order methods (see Table 1). Magnus-THRIFT 2 outperforms all other methods only for very small $\alpha < 10^{-2}$ and $T > 1$.

To investigate the scaling of the different algorithms with the system size and evolution time, we search for the lowest number of steps such that each algorithm achieves worst-case error $\|U - U_{\text{exact}}\| \leq 0.01$. For the 1D transverse-field Ising model, we scale the system size L and evolution time T together as $T = L$. The top plot of Fig. 2 shows the 2-qubit depth to get the error below threshold. For the 2D transverse-field Ising model, we fix the system size at 3×3 and only change the simulation time T when searching for the minimal circuit depth to get the error below threshold. The results are shown in the bottom of Fig. 2. In both cases, we find that the circuit depth as a function of evolution time (and system size) is well described by a power law. The power law exponents match those theoretically expected from Appendices A.1 and A.2, with the notable exception of the optimised eighth-order THRIFT formula and fourth-order Trotter formula, for which the exponents are substantially smaller. In Appendix D.1 we show these exponents as a function of the interaction strength $J = \alpha$ and discuss the results in more detail. We observe surprisingly slow growth of the circuit depth for the optimised eighth-order THRIFT formula, which appears to scale sub-linearly in the evolution time. While the small slope of opt. THRIFT 8 for the 1D case could be attributed to the model being fast-forwardable, in the 2D case we believe this is an artifact of the small system size, as the model is not believed to be fast-forwardable in general. See Appendix D.1 for more details. The specific partitions we used to implement Trotter, Omelyan et al.'s, and THRIFT algorithms for the various models we consider are discussed in Appendix C.

4.2 1D Heisenberg model with strong random fields

The second model we use for numerical tests of the THRIFT algorithms is the 1D spin- $\frac{1}{2}$ Heisenberg model with strong random fields. Unlike the 1D transverse-field Ising model, it is not exactly solvable, and we are not aware of a fast classical simulation for arbitrary times. The Hamiltonian is

$$H_{\text{Heisenberg}} = J \sum_{\langle i,j \rangle} (X_i X_j + Y_i Y_j + Z_i Z_j) + \sum_i h_i Z_i, \quad (53)$$

where the h_i are chosen uniformly random in $[-h, h]$ and X_i , Y_i , and Z_i are again the spin- $\frac{1}{2}$ operators in the respective directions. We fix $h = 1$, use the interaction strength $\alpha := J$ as the small parameter, and measure time T in units of h^{-1} . To evaluate errors, we always average over 10 different random instantiations of the field strengths

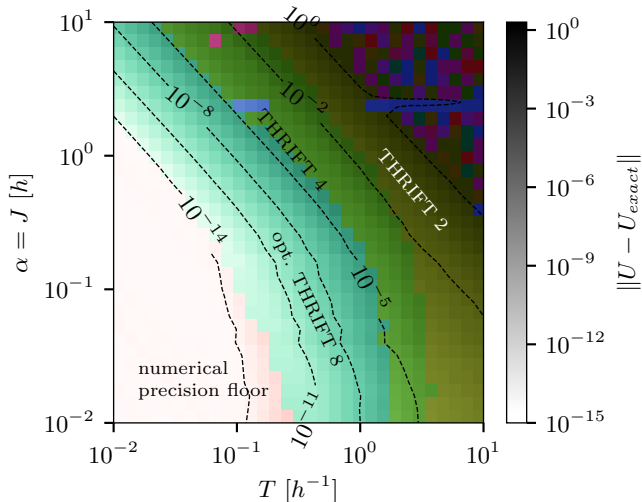


Figure 3: Landscape of the best TDS algorithm, as measured by the worst-case error $\|U - U_{\text{exact}}\|$, as a function of the relative field strength $\alpha = J/h$ and evolution time T at identical circuit depth for a 1×8 Heisenberg chain. The circuit depth is fixed to one step of optimised THRIFT 8 evolution. For the other algorithms, the number of steps is chosen to match the 2-qubit depth as closely as possible according to the 2-qubit depths shown in Table 3. The colour of each point represents the algorithm that achieves the lowest error at those values of J and T , while the brightness indicates the magnitude of the error. The isolated purple and red pixels in the THRIFT 4 and THRIFT 2 regions are artifacts of the randomness in the field strengths and running the optimised small A and eighth-order simulations with different random fields, but do not seem indicative of the general relative performance of the algorithms at these (α, T) -points.

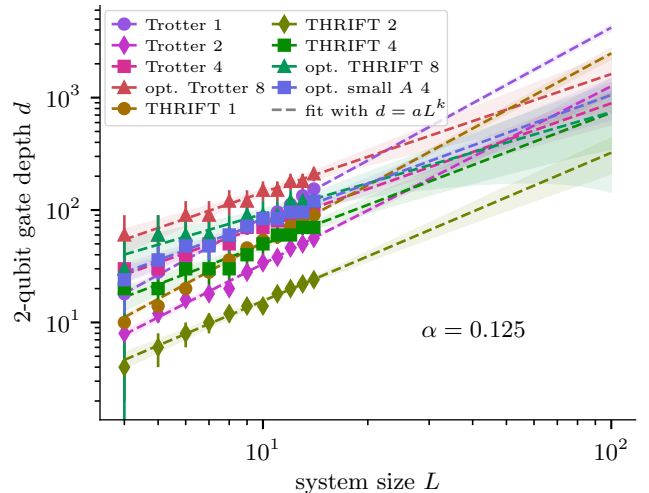


Figure 4: 2-qubit depth to achieve average infidelity $\mathbb{E}_{\{|x\rangle\}}[1 - |\langle x|U_{\text{exact}}^\dagger U|x\rangle|^2] \leq 0.01$ for the different TDS algorithms for a $1 \times L$ Heisenberg chain with field strength of $J = 1/8$ and evolution time $T = L$. Unlike Fig. 2, we use average fidelity to be able to simulate larger systems. Again, the required depths follow a power law of the form $d = aL^k$ whose parameters a and k we determine via a least-squares fit and use to extrapolate to up to $L = 100$. We report the fit parameters a and k , also for different values of α , in Fig. 11. Error bars are ± 1 step and the shaded regions are the one-sigma confidence intervals of the extrapolations.

h_i . As in the case of the transverse-field Ising model, the field part $H_0 = \sum_i h_i Z_i$ consists only of one-qubit terms, so $H_1(t)$ consists entirely of 2-qubit terms. Because simulating the Heisenberg interaction $e^{-it(X_i X_j + Y_i Y_j + Z_i Z_j)}$ already takes three CNOT gates, simulating the THRIFT gate $e^{-it(X_i X_j + Y_i Y_j + Z_i Z_j + h_i Z_i + h_j Z_j)}$ takes the same 2-qubit gate depth. Therefore, one step of any THRIFT circuit takes the same depth as one step of the corresponding Trotter circuit. See Appendix C.2.3 for more details about how we partitioned $H_{\text{Heisenberg}}$. The exact 2-qubit gate depths are shown in Table 3.

In Figs. 3 and 4 we repeat the analysis done for the transverse-field Ising model in Figs. 1 and 2 for the Heisenberg model. However, because the Heisenberg model is not integrable and average-case errors are much easier to compute than worst-case errors, we use the average infidelity as a figure of merit in Fig. 4. (Note that this may not be indicative of worst-case performance, since product formula simulations can have significantly better performance on average [35].) Similarly to the case of the transverse-field Ising model, the THRIFT methods perform better than the corresponding Trotter methods, with higher-order methods outperforming lower-order methods for smaller T and α in Fig. 3. We observe that the crossover point from one method to the next in Fig. 3 roughly happens along lines of constant αT . This is because the interaction-picture Hamiltonian $H_1(t)$ scales with α , so the relevant scale for the Trotter errors is $\alpha T/N$. For very small αT , it seems that the optimised eighth-order formula performs best in Fig. 3, but there the errors are as small as 10^{-15} , i.e., within the precision typically achieved by 64-bit floating point computations and much smaller than one could hope to achieve on real hardware. In Fig. 4 we see that the THRIFT methods always outperform the corresponding Trotter methods, and the 2-qubit gate depth to achieve

Algorithm	2-qubit gate depth	CNOT depth	# steps in Fig. 3
Trotter 1	$2N$	$6N$	15
Trotter 2	$2N + 1$	$6N + 3$	15
Trotter 4	$10N + 1$	$30N + 3$	3
optimised Trotter 8	$30N + 1$	$90N + 3$	1
THRIFT 1	$2N$	$6N + 3$	15
THRIFT 2	$2N + 1$	$6N + 3$	15
THRIFT 4	$10N + 1$	$30N + 3$	3
optimised THRIFT 8	$30N + 1$	$90N + 3$	1
optimised small A 4	$12N$	$36N$	2

Table 3: Circuit depth comparison of the different TDS algorithms investigated and shown in Fig. 3 for the 1D Heisenberg model. The first column shows the 2-qubit depth of the circuit corresponding to N Trotter steps in terms of arbitrary 2-qubit gates. The second column shows the corresponding cost in terms of CNOT gates. Finally, the third column gives the number of Trotter steps used in Fig. 3, which correspond to a fixed budget of arbitrary 2-qubit gates of 31.

average infidelity below a fixed threshold scales very similarly with T and the system size L for both methods, in broad agreement with the theory in Appendices A.1 and A.2. Figure 4 can also be directly compared to Fig. 1 in [35], which considers the same question (albeit only for Trotter and not for THRIFT methods) for the Heisenberg model at $J = 1$. That analysis finds very similar results, including matching exponents k . We present a more detailed analysis of the scaling of the circuit depth with system size and evolution time in Appendix D.2.

For this model, we did not implement the Magnus-THRIFT algorithm since we expect that it performs similarly to the 1D transverse-field Ising model case, i.e., it performs best only in a region with small α and large T . Furthermore, Magnus-THRIFT formulas of order $p > 1$ would involve unitaries acting on more than 2 qubits, resulting in a higher 2-qubit gate cost.

4.3 1D Fermi-Hubbard model with weak hopping

The last model simulated for numerical tests is the Fermi-Hubbard model on a 1D chain, which provides an example of a fermionic simulation. The Hamiltonian of the Fermi-Hubbard model is

$$H_{\text{FH}} = -t_{\text{hop}} \sum_{\langle i,j \rangle, \sigma} \left(c_{i,\sigma}^\dagger c_{j,\sigma} + c_{j,\sigma}^\dagger c_{i,\sigma} \right) + U \sum_i n_{i\uparrow} n_{i\downarrow}, \quad (54)$$

where $c_{i,\sigma}^{(\dagger)}$ are the fermionic annihilation (creation) operators on site i with spin σ and $n_{i,\sigma} = c_{i\sigma}^\dagger c_{i\sigma}$ are the corresponding number operators. The first sum runs over all edges $\langle i, j \rangle$ of the lattice and the second over all sites i .

In numerical simulations, we fix the interaction strength $U = 1$, let $\alpha := -t_{\text{hop}}$ be the small parameter, and measure time T in units of U^{-1} . To map the fermionic Hamiltonian to qubits, we use the Jordan-Wigner transformation and the same circuits developed in [36]. This results in a ladder-like interaction graph of the qubit Hamiltonian with one rung corresponding to the spin-up state on a site and one to the spin-down state on that site. As discussed in Appendix C.2.4, the interaction Hamiltonian $H_1(t)$ then consists of terms acting on four qubits, corresponding to the spin-up and spin-down states on neighbouring sites (see Fig. 9). We find numerically that time evolution with such a four-local term can be decomposed into a product of three evolutions with the hopping and three evolutions with the interaction terms for all values of T/N (the Trotter time step), t_{hop} , and U . This means that one step of any THRIFT circuit takes three times the 2-qubit gate depth of the corresponding Trotter circuit. This is in contrast to the transverse-field Ising model or Heisenberg model where the depth of THRIFT and Trotter methods is the same, because H_0 is 1-local and hence $H_1(t)$ has the same locality as H_1 . The 2-qubit gate depths per step and number of steps used in Fig. 5 are shown in Table 4.

In Figs. 5 and 6 we repeat, for 1D Fermi-Hubbard chains, the same numerical analysis that we did for the transverse-field Ising model in Figs. 1 and 2 and for the 1D Heisenberg model in Figs. 3 and 4. Because the Fermi-Hubbard model needs two qubits per site—one for each spin direction—and is not integrable, we are limited to much smaller system sizes, and for the depth scaling shown in Fig. 6, we again use the average infidelity $\mathbb{E}_{|x\rangle}[1 -$

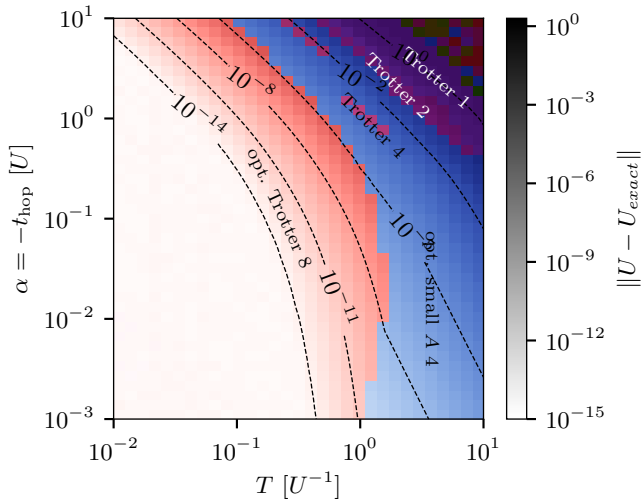


Figure 5: Landscape of the best TDS algorithm, as measured by the worst-case error $\|U - U_{\text{exact}}\|$, as a function of the hopping strength t_{hop} and evolution time T at identical circuit depth for a 1×5 Fermi-Hubbard chain. The circuit depth is fixed to 1 step of THRIFT 4 evolution. For the other algorithms, the number of steps is chosen to match the 2-qubit depth as closely as possible according to the 2-qubit depths shown in Table 4. The colour of each point represents the algorithm that achieves the lowest error at those values of t_{hop} and T , while the brightness indicates the magnitude of the error.

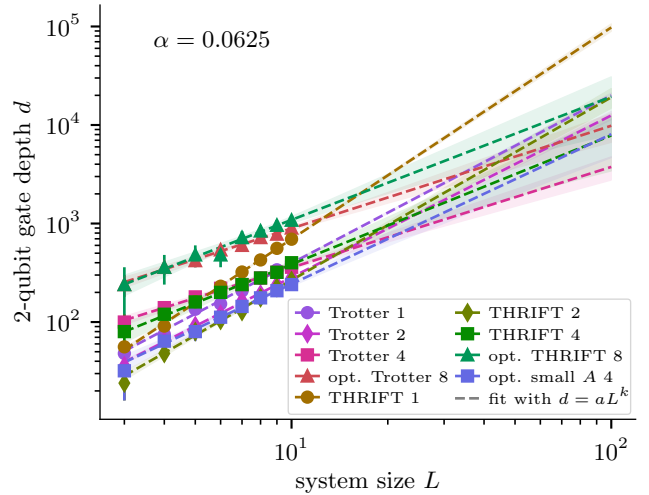


Figure 6: 2-qubit depth to achieve average infidelity $\mathbb{E}_{\{|x\rangle\}}[1 - |\langle x|U_{\text{exact}}^\dagger U|x\rangle|^2] \leq 0.01$ for the different TDS algorithms for a $1 \times L$ Fermi-Hubbard chain with an interaction strength of $t_{\text{hop}} = 1/16$ and evolution time $T = 2L$. Unlike Fig. 2, we use average fidelity to be able to simulate larger system sizes. Error bars are ± 1 step and the shaded regions are the one-sigma confidence intervals of the extrapolations. Note that, unlike the transverse-field Ising model and Heisenberg models, the extrapolation from small sizes is not as conclusive in this case, making it difficult to determine the best-performing algorithm in the 100-qubit regime.

Algorithm	2-qubit gate depth	CNOT depth	# steps in Fig. 5
Trotter 1	$3N$	$6N$	20
Trotter 2	$4N + 1$	$8N + 2$	15
Trotter 4	$20N + 1$	$40N + 2$	3
optimised Trotter 8	$60N + 1$	$120N + 2$	1
THRIFT 1	$7N$	$14N$	8
THRIFT 2	$8N + 3$	$16N + 6$	7
THRIFT 4	$40N + 3$	$80N + 6$	1
optimised THRIFT 8	$120N + 3$	$240N + 6$	N/A
optimised small A 4	$16N + 1$	$32N + 2$	3

Table 4: Circuit depth comparison of the different TDS algorithms investigated and shown in Fig. 5 for the 1D Fermi-Hubbard model. The first column shows the 2-qubit depth of the circuit corresponding to N Trotter steps in terms of arbitrary 2-qubit gates. The second column shows the corresponding cost in terms of CNOT gates. Finally, the third column gives the number of Trotter steps used in Fig. 5, which correspond to a fixed budget of arbitrary 2-qubit gates of 61. Note that, in the latter, we do not include the optimised THRIFT 8 algorithm since a single step requires deeper circuits than we allowed for Fig. 5 and increasing the circuit depth would result in most of Fig. 5 being dominated by the numerical noise floor.

$|\langle x|U_{\text{exact}}^\dagger U|x\rangle|^2$ instead of the more costly worst-case error $\|U_{\text{exact}} - U\|$. We find that within the range of T and $\alpha = -t_{\text{hop}}$ that we study, THRIFT methods rarely outperform ordinary Trotter methods, and in the regions they do (i.e., for $\alpha \leq 10^{-2}$) they are beaten by the “small A ” method of Omelyan et al. In particular, the optimised eighth-order Trotter formula of [23] and the “small A ” method of Omelyan et al. perform best out of all tested formulas for a wide range of T and α . The main reason for the poor performance of THRIFT can be traced back to the high cost of implementing the gates arising in the THRIFT decomposition, as can be seen in Table 4. Indeed, as explained in detail in Appendix C.2.4, the latter contains 4-local terms that are each implemented with 3 layers of arbitrary 2-qubit gates. Similar conclusions can be drawn by looking at the 2-qubit gate depths required to achieve a fixed average infidelity as a function of system size L and evolution time T , as shown in Fig. 6. Even for $\alpha = 1/16$, the Trotter methods have lower circuit depths than the corresponding THRIFT methods. The scaling exponents with L and T broadly agree with those expected from the theory results in Appendices A.1 and A.2 and are analysed in more detail and as a function of α in Appendix D.3.

Given the data shown in Fig. 5, we chose not to numerically study the performance of the Magnus-THRIFT algorithms for the Fermi-Hubbard model. Since THRIFT methods only become advantageous for $\alpha \leq 10^{-2}$ with respect to Trotter methods due to the more complex gates needed for the THRIFT circuits, and the second-order Magnus-THRIFT Hamiltonian $\Omega^{(2)}$ has up to 6-local terms that must be split into at least three simultaneously implementable terms (assuming the ability to implement arbitrary 6-qubit gates), we expect that the values of α for which Magnus-THRIFT becomes advantageous are rather small.

5 Discussion

Better algorithms to simulate the time dynamics of Hamiltonians with different scales have natural applications in systems where the interactions have distinct origins. We have shown both theoretically and through numerical experiments in various systems that the THRIFT algorithms can achieve better scaling than standard product formulas for Hamiltonians with different energy scales. Concretely, we consider Hamiltonians of the form $H = H_0 + \alpha H_1$, where $\alpha \ll 1$ and the norms of H_0 and H_1 are comparable. Using product formulas with a carefully chosen partition, we can achieve an $O(\alpha^2 t^k)$ error scaling for any $k \in \mathbb{N}$, which is better by a factor of α compared to the standard product formulas that do not use any structure of the Hamiltonian. We also present two algorithms to achieve scaling $O(\alpha^k t^k)$ of the approximation error. These two algorithms perform better than other formulas only in small, extreme regions of the parameter space of the systems we consider. However, such a scaling with α cannot be achieved using products of time-ordered evolutions according to the terms of the Hamiltonian, and they may achieve better performance in other applications.

While we have concentrated on the evolution generated by time-independent Hamiltonians, the methods developed in this work also generalise to time-dependent Hamiltonians satisfying the same assumptions. Consider a Hamiltonian $H(t) = H_0(t) + \alpha H_1(t)$, where $H_0(t)$ and $H_1(t)$ are time dependent and have similar norms for all times t . As before we consider α small. Using the same ideas developed in Section 2, it is possible to show that for a partition of $H_1(t) = H_1^A(t) + H_1^B(t)$, evolving the system with the approximant

$$U_{\text{apx}}(t, 0) := \mathcal{T}e^{-i \int_0^t H_0(s) ds} \mathcal{T}e^{-i \int_0^t \tilde{H}_1^A(s) ds} \mathcal{T}e^{-i \int_0^t \tilde{H}_1^B(s) ds}, \quad (55)$$

induces an error bounded by

$$\|\mathcal{T}e^{-i \int_0^t H(s) ds} - U_{\text{apx}}(t, 0)\| \leq \alpha^2 \int_0^t dv \int_0^v ds \|\tilde{H}_1^A(s), \tilde{H}_1^B(v)\|, \quad (56)$$

where $\tilde{H}_1^{A,B}(t) := \mathcal{T}e^{i \int_0^t H_0(s) ds} H_1^{A,B}(t) \mathcal{T}e^{-i \int_0^t H(s) ds}$. The main difference with respect to the time-independent case is that the evolution over a total time T cannot generically be obtained from repeating the evolution over small times, but instead must be obtained from an approximation of each time-ordered slice of the total evolution.

Although these algorithms lack the competitive scaling of other approaches not based on product formulas, it has been shown [10] that in the regime of medium sizes and time evolution scaling with the system size, standard product formulas can outperform asymptotically better algorithms. This makes our approach competitive in practical applications.

Developing algorithms that utilise the structure of the Hamiltonian to lower the cost of simulating time dynamics is crucial to make quantum computers useful sooner. In particular, our approach may help to study *dynamical phase*

transitions [37], where the behaviour of the dynamics of a system can change as a function of the parameters of the Hamiltonian. Quantum algorithms for time dynamics that fare well in particular regions of the parameter space allow exploring these questions with fewer resources, or for longer times given fixed resources and error.

Acknowledgements

We thank J. Ostmeyer for pointing out Ref. [18]. This work received funding from the European Research Council (ERC) under the European Union's Horizon 2020 research and innovation programme (grant agreement No. 817581), and from EPSRC grant EP/S516090/1, InnovateUK grant 44167, and InnovateUK grant 10032332. Andrew Childs's contribution to this publication was not part of his University of Maryland duties or responsibilities.

Appendices

A Error scaling of THRIFT

A.1 Commutator scaling

THRIFT methods approximate an interaction picture evolution unitary to p th order in t via a time-dependent product formula of the form

$$S_p(t) = e^{H_0 t} \prod_{v=1}^{\Upsilon} \prod_{\gamma=1}^{\Gamma} \mathcal{T} e^{\int_{a_{v-1}t}^{a_v t} H_{\pi_v(\gamma)}(s) ds}. \quad (57)$$

Note that, to reduce clutter and to avoid keeping track of phases, the factors of i are absorbed into the Hamiltonians in the following analysis. The results are unaffected by this choice.

Using the fact that the time dependence of the $H_\gamma(t)$ is simply unitary evolution under H_0 , this is converted back to an equivalent product formula of time-independent terms

$$S_p(t) = \prod_{v=1}^{\Upsilon} e^{(H_{\pi_v(\Upsilon)} + H_0) A_v t} e^{-H_0 A_v t} e^{(H_{\pi_v(\Upsilon-1)} + H_0) A_v t} e^{-H_0 A_v t} \dots e^{-H_0 A_v t} e^{(H_{\pi_v(1)} + H_0) A_v t}, \quad (58)$$

where $A_v = a_v - a_{v-1}$ with $a_0 = 0$. This is essentially a Trotter-style product formula of the Hamiltonian $H = H_0 + \sum_{\gamma=1}^{\Gamma} H_\gamma$ where H is decomposed into the sum

$$H = \sum_{l=1}^{2\Gamma-1} \tilde{H}_l \quad (59)$$

with $\tilde{H}_{2\gamma-1} = H_\gamma + H_0$ and $\tilde{H}_{2\gamma} = -H_0$. This product formula fits the general form used in [12],

$$S_p(t) = \prod_{v=1}^{\Upsilon} \prod_{l=1}^{2\Gamma-1} e^{\tilde{H}_{\pi_v(l)} A_v t}, \quad (60)$$

and by the main result of that work, the additive and multiplicative errors $\mathcal{A}(t)$, $\mathcal{M}(t)$, defined as

$$S_p(t) = e^{Ht} + \mathcal{A}(t) = e^{Ht} (I + \mathcal{M}(t)), \quad (61)$$

both scale as

$$\|\mathcal{A}(t)\|, \|\mathcal{M}(t)\| = O(\tilde{T}_p t^{p+1}), \quad (62)$$

where

$$\tilde{T}_p = \sum_{l_1, \dots, l_{p+1}=1}^{2\Gamma-1} \|[\tilde{H}_{l_{p+1}}, \dots, [\tilde{H}_{l_2}, \tilde{H}_{l_1}] \dots]\|, \quad (63)$$

with $\|\cdot\|$ denoting spectral norm. Expanding commutators containing terms of the form $H_\gamma + H_0$ and applying the triangle inequality, we have

$$\tilde{T}_p \leq \sum_{\gamma_1, \dots, \gamma_{p+1}=0}^{\Gamma} C_{\gamma_1, \dots, \gamma_{p+1}} \| [H_{\gamma_{p+1}}, \dots, [H_{\gamma_2}, H_{\gamma_1}] \dots] \|, \quad (64)$$

where the sum is now over $\{H_0, \dots, H_\Gamma\}$ and $C_{\gamma_1, \dots, \gamma_{p+1}}$ are constants. Setting $C_{\Gamma, p} = \max\{C_{\gamma_1, \dots, \gamma_{p+1}}\}$ (dependent only on Γ and p) and defining

$$T_p = \sum_{\gamma_1, \dots, \gamma_{p+1}=0}^{\Gamma} \| [H_{\gamma_{p+1}}, \dots, [H_{\gamma_2}, H_{\gamma_1}] \dots] \|, \quad (65)$$

we have

$$\tilde{T}_p \leq C_{\Gamma, p} T_p. \quad (66)$$

Taking Γ and p as constant, we then have for a p th-order THRIFT product formula

$$\|\mathcal{A}(t)\|, \|\mathcal{M}(t)\| = O(T_p^F t^{p+1}), \quad (67)$$

i.e., the same asymptotic scaling as a standard product formula for the decomposition into $\{H_0, \dots, H_\Gamma\}$.

A commutator treatment for average-case product formula error is given in [35]. They show that for a p th-order product formula approximating evolution under $\sum_{\gamma=0}^{\Gamma} H_\gamma$ applied to states drawn from a 1-design input ensemble, the average error in the l_2 norm is bounded asymptotically as

$$R_{l_2} = O(T_p^F t^{p+1}), \quad (68)$$

where

$$T_p^F = \sum_{\gamma_1, \dots, \gamma_{p+1}=0}^{\Gamma} \frac{1}{\sqrt{d}} \|[H_{\gamma_{p+1}}, \dots [H_{\gamma_2}, H_{\gamma_1}] \dots]\|_F, \quad (69)$$

with $\|H\|_F = \sqrt{\text{Tr}[HH^\dagger]} \leq \sqrt{d}\|H\|$ denoting the Frobenius norm. By the same argument as above for the spectral error, this asymptotic bound applies equally to THRIFT.

A.2 System size scaling for geometrically local Hamiltonians

Given a d -dimensional lattice Λ^d of n qubits with distance metric D , define a geometrically local Hamiltonian as

$$H = \sum_{Z \subset \Lambda^d} H_Z \quad (70)$$

where H_Z acts only on a finite subset of lattice sites Z and there exists a constant, finite R such that

$$\|H_Z\| \leq \begin{cases} 1 & \text{if } \text{diam}(Z) \leq R \\ 0 & \text{if } \text{diam}(Z) > R, \end{cases} \quad (71)$$

where $\text{diam}(Z) = \max\{D(i, j) : i, j \in Z\}$ is the maximum distance between any two points in Z .

Lemma 8. *A p th-order product formula approximating evolution under a Hamiltonian $H = \sum_{\gamma=1}^{\Gamma} H_\gamma$, where all H_γ are geometrically local on a lattice of n qubits, has additive and multiplicative error with the following asymptotic scaling:*

$$\|\mathcal{A}(t)\|, \|\mathcal{M}(t)\| = O(nt^{p+1}). \quad (72)$$

Proof. By the results in [12] we have the bound

$$\|\mathcal{A}(t)\|, \|\mathcal{M}(t)\| = O\left(\sum_{\gamma_1, \dots, \gamma_{p+1}=1}^{\Gamma} \|W_{\gamma_1, \dots, \gamma_{p+1}}\| t^{p+1}\right), \quad (73)$$

where $W_{\gamma_1, \dots, \gamma_{p+1}} = [H_{\gamma_{p+1}}, \dots [H_{\gamma_2}, H_{\gamma_1}] \dots]$. As any given H_γ is geometrically local it can be written as in Eq. (70) as

$$H = \sum_{Z \subset \Lambda^d} H_{\gamma, Z}, \quad (74)$$

where the $H_{\gamma, Z}$ act on subsets Z of maximum diameter R . For lattice site i let us define

$$H_\gamma^i := \sum_{Z \ni i} \frac{1}{|Z|} H_{\gamma, Z}, \quad (75)$$

i.e., the sum of all local terms in H_γ that act on site i , each divided by the size of their support set; this accounts for multi-counting and means that we can write

$$H_\gamma = \sum_{i \in \Lambda^d} H_\gamma^i. \quad (76)$$

For each H_γ^i we have $\|H_\gamma^i\| \leq C$ for some constant C dependent on R and d . We may now write

$$W_{\gamma_1, \dots, \gamma_{p+1}} = \sum_{i_1, \dots, i_{p+1} \in \Lambda^d} [H_{\gamma_{p+1}}^{i_{p+1}}, \dots, [H_{\gamma_2}^{i_2}, H_{\gamma_1}^{i_1}] \dots]. \quad (77)$$

We can simplify this expression by omitting terms that are zero due to lack of shared support. The commutator $[H_{\gamma_2}^{i_2}, H_{\gamma_1}^{i_1}]$ vanishes if i_2 is more than $2R$ away from i_1 as no part of the two arguments will overlap. Furthermore, assuming the inside commutator is nonzero, $[H_{\gamma_3}^{i_3}, [H_{\gamma_2}^{i_2}, H_{\gamma_1}^{i_1}]]$ vanishes if i_3 is more than $3R$ away from i_1 , because at that distance, $H_{\gamma_3}^{i_3}$ only overlaps with the parts of $H_{\gamma_2}^{i_2}$ that do not overlap with $H_{\gamma_1}^{i_1}$. By similar logic, i_4 must be within $4R$ of i_1 , and so on. We can then reduce the sum to

$$W_{\gamma_1, \dots, \gamma_{p+1}} = \sum_{i_{p+1}: D(i_{p+1}, i_1) \leq (p+1)R} \dots \sum_{i_2: D(i_2, i_1) \leq 2R} \sum_{i_1 \in \Lambda^d} [H_{\gamma_{p+1}}^{i_{p+1}}, \dots, [H_{\gamma_2}^{i_2}, H_{\gamma_1}^{i_1}] \dots]. \quad (78)$$

The number of lattice points within a fixed distance of a given point is constant, so the sum over $\|W_{\gamma_1, \dots, \gamma_{p+1}}\|$ in Eq. (73) simply reduces to a sum of constants over the points $i_1 \in \Lambda^d$, which is proportional to the number of lattice points n . The result follows. \square

Corollary 9. *For a p th-order product formula for a Hamiltonian H as described above, to simulate evolution for time t with accuracy ϵ , it suffices to use r iterations of the product formula, where*

$$r = O\left(\frac{n^{1/p}}{\epsilon^{1/p}} t^{1+1/p}\right). \quad (79)$$

The above results apply equally to THRIFT product formulas, using either the error scaling given in Eq. (62) or in Eq. (67). Furthermore, linear scaling of the spectral error with system size also applies to the average-case error by a similar argument.

A.3 Limits on error scaling in α for time-dependent product formulas

In this section we establish limitations on how well time-dependent product formulas can approximate Hamiltonian dynamics as a function of α , a scaling factor for the Hamiltonian. Such an evolution is obtained in THRIFT when approximating the time-dependent part of an interaction-picture evolution operator via a time-dependent product formula. In particular, the Hamiltonian in this time-dependent part is scaled by α , so these results provide limitations on the α -dependence of THRIFT.

Theorem 10. *For a Hamiltonian of the form*

$$H(t) = \sum_{\gamma=1}^{\Gamma} \alpha H_\gamma(t), \quad (80)$$

consider a time-dependent product formula of the form

$$S(t) = \prod_{v=1}^{\Upsilon} \prod_{\gamma=1}^{\Gamma} \mathcal{T} e^{\int_{a_{v-1}t}^{a_v t} \alpha H_{\pi_v(\gamma)}(s) ds}, \quad (81)$$

where π_v are permutations of the indices γ and a_v are real numbers defining time intervals $[a_{v-1}t, a_v t]$. There is no such product formula for which

$$\left\| S(t) - \mathcal{T} e^{\int_0^t \alpha H(s) ds} \right\| = O(\alpha^k) \quad (82)$$

for $k > 2$ and $t \neq 0$.

Proof. We expand the terms of Eq. (82) into integral series, yielding Taylor series in α that can be compared term-by-term. Up to second order, the Dyson series for evolution under $H(t)$ over the interval $[0, t]$ is

$$\mathcal{T} e^{\int_0^t \alpha H(s) ds} = 1 + \alpha \int_0^t ds_1 \sum_{\gamma} H_\gamma(s_1) + \alpha^2 \int_0^t ds_1 \int_0^{s_1} ds_2 \sum_{\gamma_1, \gamma_2} H_{\gamma_1}(s_1) H_{\gamma_2}(s_2) + O(\alpha^3). \quad (83)$$

Expanding each time-ordered integral in $S(t)$ and collecting powers of α gives the second-order expansion

$$\begin{aligned}
S(t) &= 1 + \alpha \sum_v \int_{a_{v-1}t}^{a_v t} ds_1 \sum_{\gamma} H_{\gamma}(s_1) \\
&+ \alpha^2 \sum_v \int_{a_{v-1}t}^{a_v t} ds_1 \int_{a_{v-1}t}^{s_1} ds_2 \sum_{\gamma} H_{\gamma}(s_1) H_{\gamma}(s_2) \\
&+ \alpha^2 \sum_v \int_{a_{v-1}t}^{a_v t} ds_1 \int_{a_{v-1}t}^{a_v t} ds_2 \sum_{\gamma_1 < \gamma_2} H_{\pi_v(\gamma_1)}(s_1) H_{\pi_v(\gamma_2)}(s_2) \\
&+ \alpha^2 \sum_{v>u} \int_{a_{v-1}t}^{a_v t} ds_1 \int_{a_{u-1}t}^{a_u t} ds_2 \sum_{\gamma_1, \gamma_2} H_{\gamma_1}(s_1) H_{\gamma_2}(s_2) + O(\alpha^3).
\end{aligned} \tag{84}$$

Combining integrals with matching boundaries and using the fact that $v > u$, we may rewrite this as

$$\begin{aligned}
S(t) &= 1 + \alpha \int_{a_0 t}^{a_{\Gamma} t} ds_1 \sum_{\gamma} H_{\gamma}(s_1) \\
&+ \alpha^2 \int_{a_0 t}^{a_{\Gamma} t} ds_1 \int_{a_0 t}^{s_1} ds_2 \sum_{\gamma} H_{\gamma}(s_1) H_{\gamma}(s_2) \\
&+ \alpha^2 \sum_v \int_{a_{v-1}t}^{a_v t} ds_1 \int_{a_{v-1}t}^{a_v t} ds_2 \sum_{\gamma_1 < \gamma_2} H_{\pi_v(\gamma_1)}(s_1) H_{\pi_v(\gamma_2)}(s_2) \\
&+ \alpha^2 \sum_v \int_{a_0 t}^{a_v t} ds_1 \int_{a_0 t}^{a_{v-1}t} ds_2 \sum_{\gamma_1 \neq \gamma_2} H_{\gamma_1}(s_1) H_{\gamma_2}(s_2) + O(\alpha^3).
\end{aligned} \tag{85}$$

Clearly, for $S(t)$ to approximate evolution under $H(t)$ over $[0, t]$ to first order in α , we must have $a_0 = 0$ and $a_{\Gamma} = 1$. Then we find the following expression for the difference between $S(t)$ and the ideal evolution:

$$\begin{aligned}
S(t) - \mathcal{T}e^{\int_0^t \alpha H(s) ds} &= \alpha^2 \sum_v \int_{a_{v-1}t}^{a_v t} ds_1 \int_{a_{v-1}t}^{a_v t} ds_2 \sum_{\gamma_1 < \gamma_2} H_{\pi_v(\gamma_1)}(s_1) H_{\pi_v(\gamma_2)}(s_2) \\
&+ \alpha^2 \sum_v \int_0^{a_v t} ds_1 \int_0^{a_{v-1}t} ds_2 \sum_{\gamma_1 \neq \gamma_2} H_{\gamma_1}(s_1) H_{\gamma_2}(s_2) \\
&- \alpha^2 \int_0^t ds_1 \int_0^{s_1} ds_2 \sum_{\gamma_1 \neq \gamma_2} H_{\gamma_1}(s_1) H_{\gamma_2}(s_2) + O(\alpha^3).
\end{aligned} \tag{86}$$

By inserting

$$0 = \alpha^2 \sum_v \int_{a_{v-1}t}^{a_v t} ds_1 \int_{a_{v-1}t}^{s_1} ds_2 \sum_{\gamma_1 < \gamma_2} (H_{\pi_v(\gamma_2)}(s_1) H_{\pi_v(\gamma_1)}(s_2) - H_{\pi_v(\gamma_2)}(s_1) H_{\pi_v(\gamma_1)}(s_2)), \tag{87}$$

doing some algebra, and relabelling integral variables where needed, we finally arrive at a more compact form for the error at second order, namely

$$\begin{aligned}
S(t) - \mathcal{T}e^{\int_0^t \alpha H(s) ds} &= \Delta \alpha^2 + O(\alpha^3) \\
\text{with } \Delta &= \sum_v \int_{a_{v-1}t}^{a_v t} ds_1 \int_{s_1}^{a_v t} ds_2 \sum_{\gamma_1 < \gamma_2} [H_{\pi_v(\gamma_1)}(s_1), H_{\pi_v(\gamma_2)}(s_2)].
\end{aligned} \tag{88}$$

The question then becomes: is there a generic set of parameters $\{a_v\}$ and $\{\pi_v\}$ such that Δ vanishes?¹ Relabelling

¹Technically, for the error to agree up to second order, Δ only needs to be $O(\alpha^3)$, but for a generic set of parameters there can be no α dependence.

category	function definition	non-zero region
$\Pi_{\gamma_1, \gamma_2}^v$ even $a_{v-1}t < a_v t$	$f_{\gamma_1, \gamma_2}^v(s_1, s_2) = \begin{cases} 1 & : a_{v-1}t < s_1 < s_2 < a_v t \\ 0 & : \text{otherwise} \end{cases}$	
$\Pi_{\gamma_1, \gamma_2}^v$ even $a_v t < a_{v-1}t$	$f_{\gamma_1, \gamma_2}^v(s_1, s_2) = \begin{cases} 1 & : a_v t < s_2 < s_1 < a_{v-1}t \\ 0 & : \text{otherwise} \end{cases}$	
$\Pi_{\gamma_1, \gamma_2}^v$ odd $a_{v-1}t < a_v t$	$f_{\gamma_1, \gamma_2}^v(s_1, s_2) = \begin{cases} -1 & : a_{v-1}t < s_2 < s_1 < a_v t \\ 0 & : \text{otherwise} \end{cases}$	
$\Pi_{\gamma_1, \gamma_2}^v$ odd $a_v t < a_{v-1}t$	$f_{\gamma_1, \gamma_2}^v(s_1, s_2) = \begin{cases} -1 & : a_v t < s_1 < s_2 < a_{v-1}t \\ 0 & : \text{otherwise} \end{cases}$	

Table 5: The form of f_{γ_1, γ_2}^v depends on the parity of $\Pi_{\gamma_1, \gamma_2}^v$, i.e., whether it switches 1 and 2, and whether $a_{v-1}t < a_v t$. All four possibilities are shown, along with a visualisation of their non-zero region as a shaded area on the s_1 - s_2 plane. Blue shading with a “+” indicates a value of +1 and, likewise, red with a “-” a value of -1.

variables and using the antisymmetry of the commutator, we may write

$$\Delta = \sum_v \sum_{\gamma_1 < \gamma_2} \mathcal{S}(\pi_v, \gamma_1, \gamma_2) \int_{a_{v-1}t}^{a_v t} ds_{\Pi_{\gamma_1, \gamma_2}^v(1)} \int_{s_{\Pi_{\gamma_1, \gamma_2}^v(1)}}^{a_v t} ds_{\Pi_{\gamma_1, \gamma_2}^v(2)} [H_{\gamma_1}(s_1), H_{\gamma_2}(s_2)] \quad (89)$$

where the function $\mathcal{S}(\pi_v, \gamma_1, \gamma_2)$ is -1 if the permutation π_v switches the order of γ_1, γ_2 and +1 otherwise, and $\Pi_{\gamma_1, \gamma_2}^v$ is a permutation of the indices 1 and 2 defined as

$$\Pi_{\gamma_1, \gamma_2}^v((1, 2)) = \begin{cases} (1, 2) & \text{if } \pi_v((\gamma_1, \gamma_2)) = (\gamma_1, \gamma_2), \\ (2, 1) & \text{if } \pi_v((\gamma_1, \gamma_2)) = (\gamma_2, \gamma_1). \end{cases} \quad (90)$$

We may further rewrite this as

$$\Delta = \sum_{\gamma_1 < \gamma_2} \iint_{[t_{\min}, t_{\max}]^2} ds_1 ds_2 \sum_v f_{\gamma_1, \gamma_2}^v(s_1, s_2) [H_{\gamma_1}(s_1), H_{\gamma_2}(s_2)], \quad (91)$$

where t_{\min} and t_{\max} are the minimum and maximum values of $\{a_v t\}_{v=1}^{\Upsilon}$ and f_{γ_1, γ_2}^v are functions that are zero everywhere except for the corresponding region of integration in Eq. (89) where they take the value of $\mathcal{S}(\pi_v, \gamma_1, \gamma_2)$. The possible forms of these functions are visualised in Table 5. For Δ to vanish, each term in the sum over $\gamma_1 < \gamma_2$ must vanish. Furthermore, for arbitrary time-dependent Hamiltonians, this requires that the respective sums $\sum_v f_{\gamma_1, \gamma_2}^v(s_1, s_2)$ vanish for all s_1, s_2 . By inspection of the forms of these functions in Table 5, it is clear that this requires every time step $(a_{v-1}t, a_v t)$ to have a step of the same size in the reverse direction, meaning that Δ only vanishes for evolution over zero time. Theorem 10 then follows. \square

In fact, Theorem 10 holds even with the further restriction that the time-dependence of the Hamiltonian arises via conjugation by some fixed Hamiltonian dynamics, as in the case of THRIFT.

Theorem 11. *Theorem 10 also holds for the restricted case where $H_\gamma(t) = e^{H_0 t} H_\gamma(0) e^{-H_0 t}$ for some fixed H_0 .*

We show this by adapting the above proof of [Theorem 10](#). The sum over $\gamma_1 < \gamma_2$ must still vanish term-wise, so let us simplify by analysing the $\gamma_1 = 1, \gamma_2 = 2$ term, denoting it $T(H_1, H_2)$. Let us simplify further by writing the sum over $f_{1,2}^v$ as a single function F and relabelling $s_1 \rightarrow x, s_2 \rightarrow y$, so we have

$$T(H_1, H_2) = \iint_{S^2} dx dy F(x, y) [H_1(x), H_2(y)], \quad (92)$$

where $S := [t_{\min}, t_{\max}]$. We have

$$H_1(t) = e^{H_0 t} H_1(0) e^{-H_0 t}, \quad H_2(t) = e^{H_0 t} H_2(0) e^{-H_0 t}. \quad (93)$$

Lemma 12. *If $T(H_1, H_2) = 0$ for any H_1 with $[H_0, H_1(0)] \neq 0$, then $T(H'_1, H_2) = 0$ for any H'_1 with $[H_0, H'_1(0)] = 0$.*

Proof. For H'_1 such that $[H_0, H'_1(0)] = 0$ define $H''_1(x) = H'_1(x) + A(x)$ where $A(x)$ is some operator-valued function with $[H_0, A(0)] \neq 0$. Then by linearity we have

$$T(H'_1, H_2) = T(H''_1, H_2) + T(A, H_2) = 0. \quad (94)$$

As $T(A, H_2) = 0$ by hypothesis, we have $T(H'_1, H_2) = 0$. \square

Lemma 13. *If $T(H_1, H_2) = 0$ for any H_1, H_2 , then for all $k \in \mathbb{N}$,*

$$\iint_{S^2} dx dy F(x, y) x^k = \iint_{S^2} dx dy F(x, y) y^k = 0. \quad (95)$$

Proof. Let $[H_1(0), H_0] = 0$ and $H_0 = \lambda H'_0$. Expand Δ as a power series in λ to get

$$\Delta = \sum_k \frac{1}{k!} \iint_{S^2} dx dy F(x, y) [H_1, \text{ad}_{H'_0}^k H_2] y^k \lambda^k = 0 \quad (96)$$

where $\text{ad}_A B = [A, B]$ and we write $H_1(0)$ as H_1 , likewise for H_2 . This series must vanish term-by-term with λ , so we have

$$[H_1, \text{ad}_{H'_0}^k H_2] \iint_{S^2} dx dy F(x, y) y^k = 0 \quad \forall k \in \mathbb{N}. \quad (97)$$

Let H'_0, H_1, H_2 be Paulis that pairwise anticommute except H_0 and H_1 . Then $\text{ad}_{H'_0}^k H_2 = 2^k H_0'^k H_2$, meaning $[H_1, \text{ad}_{H'_0}^k H_2] \neq 0$ for all $k \in \mathbb{N}$. For $T(H_1, H_2) = 0$ to hold in general, the above integral must then vanish for all k . The same argument applies for x . \square

Lemma 14. *If for all $k \in \mathbb{N}$,*

$$\int_{[a,b]} dx f(x) x^k = 0, \quad (98)$$

then

$$f(x) = 0 \quad \text{almost everywhere in } [a, b], \quad (99)$$

i.e., it is nonzero on only a measure-zero subset of $[a, b]$.

Proof. The following proof is reproduced from [\[38\]](#) in more detail.

Let $f(x)$ be integrable over the interval $[a, b]$ and have the property that $\int_{[a,b]} dx f(x) x^k = 0$ for all $k \in \mathbb{N}$. It follows that $\int_{[a,b]} dx f(x) p(x) = 0$ for any polynomial p . The polynomials are dense in the set of continuous functions on $[a, b]$, so it also follows that for any continuous function g , $\int_{[a,b]} dx f(x) g(x) = 0$.

Assume now that f is not zero almost everywhere. Then the set $\{x : f(x) > 0\}$ has finite measure. One can then find δ such that $\{x : f(x) > \delta\}$ has finite measure. By the regularity of the Lebesgue measure, one can choose

a compact set K and open set V such that $K \subset \{x : f(x) > \delta\} \subset V$ and the measure of $V \setminus K$ is arbitrarily small. Let g be a continuous function such that $0 \leq g(x) \leq 1$ which is equal to 1 on K and 0 outside of V . Then we have

$$\left| \int_{[a,b]} dxg(x)f(x) \right| = \left| \int_V dxg(x)f(x) \right| = \left| \int_K dxg(x)f(x) + \int_{V \setminus K} dxg(x)f(x) \right|. \quad (100)$$

By the (reverse) triangle inequality, we have

$$\begin{aligned} \left| \int_{[a,b]} dxg(x)f(x) \right| &\geq \left| \int_K dxg(x)f(x) \right| - \left| \int_{V \setminus K} dxg(x)f(x) \right| \\ &\geq \left| \int_K dxg(x)f(x) \right| - \int_{V \setminus K} dx|g(x)f(x)|. \end{aligned} \quad (101)$$

Now as g is 1 on K and $g < 1$ for some region on V , we have

$$\left| \int_{[a,b]} dxg(x)f(x) \right| \geq \left| \int_K dx f(x) \right| - \int_{V \setminus K} dx|f(x)|. \quad (102)$$

As noted before, $f > \delta$ on K , so

$$\left| \int_{[a,b]} dxg(x)f(x) \right| \geq \delta m(K) - \int_{V \setminus K} dx|f(x)| \quad (103)$$

where $m(K) > 0$ is the measure of K . Since $V \setminus K$ can be made arbitrarily small, we can take the right-hand side of the inequality to be positive, meaning that $\left| \int_{[a,b]} dxg(x)f(x) \right|$ for some continuous g , which is a contradiction. \square

Corollary 15. *If for all $k \in \mathbb{N}$,*

$$\iint_{S^2} dx dy F(x, y) x^k = 0, \quad (104)$$

then as a function of x ,

$$\int_S dy F(x, y) = 0 \quad \text{almost everywhere in } S. \quad (105)$$

The same holds when y and x are exchanged.

Proof. Set

$$f(x) = \int_S dy F(x, y) \quad (106)$$

and $[a, b] = S$. The result follows immediately from [Lemma 14](#). \square

Lemma 16. *If $T(H_1, H_2) = 0$ for all $H_0, H_1(x), H_2(y)$ as defined above, then $a_{\Upsilon t} = a_0 t$.*

Proof. Assume $a_{\Upsilon t} \neq a_0 t$. The intervals $[a_{v-1}t, a_v t]$ are “steps” in a path from $a_0 t$ to $a_{\Upsilon t}$, so any point in $S \setminus \{a_v t\}$ is contained within an odd number of these intervals as the path must cross it an odd number of times. Consider the open interval $(a_v t, a'_v t)$ where $a'_v = \min\{a_u : a_u > a_v\}$. Any point in this set is contained in the same set of “step” intervals. There must exist a v for which $(a_v t, a'_v t) \cap [a_0 t, a_{\Upsilon t}] \neq \emptyset$, so there exists a finite-measure set of points that are all contained within the same set of steps M where $|M|$ is odd.

As $F(x, y)$ is a sum of the functions in [Table 5](#), we can see that for a point x' in this set, the integral $\int_S dy F(x', y)$ takes the form

$$\int_S dy F(x', y) = \sum_{v: [a_{v-1}t, a_v t] \in M} s_v(x' - T_v) \quad (107)$$

where $s_v \in \{\pm 1\}$ and $T_v \in \{a_{v-1}t, a_v t\}$. Consider now the integral for $x' + c \in (a_v t, a'_v t)$,

$$\begin{aligned} \int_S dy F(x' + c, y) &= \sum_{v: [a_{v-1}t, a_v t] \in M} s_v (x' + c - T_v) \\ &= \sum_{v: [a_{v-1}t, a_v t] \in M} s_v (x' - T_v) + \sum_{v: [a_{v-1}t, a_v t] \in M} s_v c. \end{aligned} \quad (108)$$

As $|M|$ is odd and s_v are signs,

$$\left| \sum_{v: [a_{v-1}t, a_v t] \in M} s_v c \right| \geq 1, \quad (109)$$

and $\int_S dy F(x, y)$ is non-zero on a finite measure set, contradicting [Corollary 15](#). \square

We are now ready to prove [Theorem 11](#).

Proof of Theorem 11. Recall that for the product formula in [Eq. \(81\)](#) to agree up to α^2 for arbitrary times, the quantity

$$\Delta = \sum_{\gamma_1 < \gamma_2} \iint_{S^2} ds_1 ds_2 F(s_1, s_2) [H_{\gamma_1}, H_{\gamma_2}] \quad (110)$$

must vanish. This sum must vanish term-wise, so it suffices to consider the $\gamma_1 = 1, \gamma_2 = 2$ case. By [Lemma 16](#), this term may only vanish if $a_0 t = a_T t$. As argued in the proof of [Theorem 10](#), first-order agreement requires $a_0 = 0$ and $a_T = 1$, so second-order agreement can only hold if $t = 0$. \square

B Convergence of Magnus expansion

A simple proof of the convergence of the Magnus expansion is given in [\[29\]](#). Here we reproduce it for completeness. The first ingredient is the following lemma.

Lemma 17 (A Bihari-type inequality [\[29\]](#)). *Let $h, v \in C(0, T)$ (where $C(0, T)$ denotes functions with a continuous first derivative on the interval $[0, T]$) be integrable positive functions and let $g \in C(0, T)$ be a non-decreasing positive function. Then*

$$h(x) \leq \int_0^x v(s)g(h(s))ds \quad (111)$$

for $x \in [0, T]$ implies that $h(x) \leq \int_0^x v(s)g(h(s))ds \leq G^{-1}(\int_0^x v(s)ds)$, where G^{-1} is the inverse function of $G(s) = \int_0^s \frac{ds}{g(s)}$.

Proof. Define $f(x) := \int_0^x v(x)g(h(x))dx$, so $\frac{df}{dx} = v(x)g(h(x))$. Using [Eq. \(111\)](#), $h \leq f$, which implies $g(h(x)) \leq g(f(x))$ as g is non-decreasing. Therefore $\frac{df}{dx} \leq v(x)g(f(x))$. Dividing by g and integrating by substitution, we have

$$\int_0^{f(t)} \frac{ds}{g(s)} \leq \int_0^t v(x)dx \quad \Rightarrow \quad G(f(t)) \leq \int_0^t v(x)dx. \quad (112)$$

Applying the inverse of G and using $h \leq f$ completes the proof. \square

Theorem 18. *The Magnus expansion $\Omega(t)$, defined by $\mathcal{T} e^{-i\alpha \int_0^t H_1(s)ds} = e^{\Omega(t)}$ and the series in [Eq. \(17\)](#), converges for $|\alpha| \int_0^t \|H_1(s)\|ds \leq 1.08687\dots$*

Proof. Starting from the definition of the Magnus operator [Eq. \(17\)](#), the triangle inequality gives

$$\|\Omega(t)\| \leq |\alpha| \int_0^t \sum_{k=0}^{\infty} \frac{|b_k|}{k!} (2\|\Omega(s)\|)^k \|H_1(s)\|ds = |\alpha| \int_0^t g(2\|\Omega(s)\|) \|H_1(s)\|ds. \quad (113)$$

As g is a nondecreasing positive function in the interval $[0, 2\pi)$, we can apply [Lemma 17](#), giving

$$\|\Omega(t)\| \leq \frac{1}{2}G^{-1}\left(2|\alpha| \int_0^t \|H_1(s)\| ds\right). \quad (114)$$

This implies that $\|\Omega(t)\|$ is bounded as long as

$$|\alpha| \int_0^t \|H_1(s)\| ds \leq \frac{1}{2}G(2\pi) = \frac{1}{2} \int_0^{2\pi} \frac{ds}{2 + \frac{x}{2}(1 - \cot(x/2))} = 1.08687\dots, \quad (115)$$

as claimed. \square

The proof of the Magnus-THRIFT approximation theorem ([Theorem 4](#)) uses [Lemma 3](#), which we now prove.

Lemma 19. For $1 \leq l$, $\|\tilde{\Omega}_l(t)\| \leq \frac{1}{2}x_l(2 \int_0^t \|H_1(s)\| ds)^l$, where x_l is the coefficient of s^l in the expansion of $G^{-1}(s) = \sum_{m=1}^{\infty} x_m s^m$, the inverse function of $G(s) = \int_0^s (2 + \frac{x}{2}(1 - \cot(x/2)))^{-1} dx$.

Proof. We proceed by induction. First, as $\tilde{\Omega}_1(t) = -i \int_0^t H_1(s) ds$, we have

$$\|\tilde{\Omega}_1(t)\| \leq \int_0^t \|H_1(s)\| ds = \frac{x_1}{2} \left(2 \int_0^t \|H_1(s)\| ds\right) \quad (116)$$

with $x_1 = 1$. The induction hypothesis is $\|\tilde{\Omega}_l(t)\| \leq \frac{1}{2}x_l(2 \int_0^t \|H_1(s)\| ds)^l$ for $1 \leq l \leq n$. To prove the induction step, we integrate [Eq. \(18\)](#) and use the triangle inequality, leading to

$$\begin{aligned} \|\tilde{\Omega}_{n+1}(t)\| &\leq \sum_{j=1}^n \frac{|b_j|}{j!} \sum_{\substack{k_1+k_2+\dots+k_j=n \\ k_1, k_2, \dots, k_j \geq 1}} \int_0^t 2^j \prod_{m=1}^j \|\tilde{\Omega}_{k_m}(s)\| \|H_1(s)\| ds, \\ &= \sum_{j=1}^n \frac{|b_j|}{j!} \int_0^t 2^j \hat{B}_{n,j}(\|\tilde{\Omega}_1(s)\|, \dots, \|\tilde{\Omega}_{n-j+1}(s)\|) \|H_1(s)\| ds, \end{aligned} \quad (117)$$

where we have introduced the ordinary Bell polynomials [[39](#), [40](#)], defined by

$$\hat{B}_{n,j}(x_1, x_2, \dots, x_{n-j+1}) := \frac{1}{n!} \frac{\partial^n}{\partial \alpha^n} \left(\sum_{k=1}^{\infty} \alpha^k x_k \right) \Big|_{\alpha=0} = \sum_{\substack{k_1+k_2+\dots+k_j=n \\ k_1, k_2, \dots, k_j \geq 1}} \prod_{m=1}^j x_{k_m}. \quad (118)$$

Using the induction hypothesis on [Eq. \(117\)](#) and that $\hat{B}_{n,j}(r x_1, r^2 x_2, \dots, r^{n-k+1} x_{n-k+1}) = r^n \hat{B}_{n,j}(x_1, x_2, \dots, x_{n-k+1})$, which follows from the definition [Eq. \(118\)](#), we have

$$\|\tilde{\Omega}_{n+1}(t)\| \leq \left(\int_0^t \left(2 \int_0^s \|H_1(y)\| dy \right)^n \|H_1(s)\| ds \right) \sum_{j=1}^n \frac{|b_j|}{j!} \hat{B}_{n,j}(x_1, \dots, x_{n-j+1}), \quad (119)$$

$$= \left(\frac{1}{2} \int_0^t \frac{d}{ds} \left(\frac{2 \int_0^s \|H(x)\| dx}{n+1} \right)^{n+1} ds \right) \sum_{j=1}^n \frac{|b_j|}{j!} \hat{B}_{n,j}(x_1, \dots, x_{n-j+1}) \quad \text{using the chain rule,} \quad (120)$$

$$= \frac{(2 \int_0^t \|H(x)\| dx)^{n+1}}{n+1} \frac{1}{2} \sum_{j=1}^n \frac{|b_j|}{j!} \hat{B}_{n,j}(x_1, \dots, x_{n-j+1}) \quad \text{using the fundamental theorem of calculus.} \quad (121)$$

To finish the proof, we show that the factor $\frac{1}{(n+1)} \sum_{j=1}^n \frac{|b_j|}{j!} \hat{B}_{n,j}(x_1, \dots, x_{n-j+1})$ corresponds to the coefficient of z^{n+1} in the series expansion $G^{-1}(z) = \sum_{m=1}^{\infty} z^m x_m$, given that $\{x_j\}_{j=1}^n$ are also coefficients of G^{-1} . That can be shown as follows:

$$X_{n+1} := \frac{1}{n+1} \sum_{j=1}^n \frac{|b_j|}{j!} \hat{B}_{n,j}(x_1, \dots, x_{n-j+1}) = \frac{1}{(n+1)!} \sum_{j=1}^n |b_j| B_{n,j}(1!x_1, 2!x_2, \dots, (n-j+1)!x_{n-k+1}) \quad (122)$$

where we used the relation

$$\frac{n!}{j!} \hat{B}_{n,j}(x_1, \dots, x_{n-j+1}) = B_{n,j}(1!x_1, 2!x_2, \dots, (n-j+1)!x_{n-k+1}) \quad (123)$$

between the ordinary Bell polynomials $\hat{B}_{n,k}$ and the exponential Bell polynomials $B_{n,k}$ [40]. Now note that $G^{-1}(z) = \sum_{n=1}^{\infty} z^n x_n$ implies $\frac{d^n G^{-1}(0)}{dz^n} = n!x_n$, so we can write Eq. (122) as

$$\begin{aligned} X_{n+1} &= \frac{1}{(n+1)!} \sum_{j=1}^n |b_j| B_{n,j} \left(\frac{dG^{-1}(0)}{dz}, \frac{d^2 G^{-1}(0)}{dz^2}, \dots, \frac{d^{n-j+1} G^{-1}(0)}{dz^{n-j+1}} \right), \\ &= \frac{1}{(n+1)!} \sum_{j=1}^n \frac{d^j g(0)}{dz^j} B_{n,j} \left(\frac{dG^{-1}(0)}{dz}, \frac{d^2 G^{-1}(0)}{dz^2}, \dots, \frac{d^{n-j+1} G^{-1}(0)}{dz^{n-j+1}} \right), \end{aligned} \quad (124)$$

with $g(z) = \sum_{j=0}^{\infty} \frac{|b_j|}{j!} z^j = 2 + \frac{z}{2}(1 - \cot(z/2))$. Finally, using the derivative rule for inverse functions $\frac{dG^{-1}(z)}{dz} = \frac{1}{G'(G^{-1}(z))}$ and the definition of $G(z) = \int_0^z (g(s))^{-1} ds$, we have $\frac{dG^{-1}(z)}{dz} = g(G^{-1}(z))$. In general,

$$\frac{d^{n+1}}{dz^{n+1}} (G^{-1}(z)) = \frac{d^n}{dz^n} (g(G^{-1}(z))) = \sum_{k=1}^n \frac{d^k}{dz^k} (g(G^{-1}(z))) B_{n,k} \left(\frac{dG^{-1}(z)}{dz}, \frac{d^2 G^{-1}(z)}{dz^2}, \dots, \frac{d^{n-k+1} G^{-1}(z)}{dz^{n-k+1}} \right) \quad (125)$$

where we have used Faà di Bruno's identity for the generalised chain rule [41]. Comparing Eq. (124) and Eq. (125), we find

$$X_{n+1} = \frac{1}{(n+1)!} \frac{d^{n+1}}{dz^{n+1}} (G^{-1}(0)), \quad (126)$$

which is by definition x_{n+1} . Going back to Eq. (121), this implies

$$\|\tilde{\Omega}_{n+1}(t)\| \leq \frac{x_{n+1}}{2} \left(2 \int_0^t \|H(x)\| dx \right)^{n+1} = \frac{1}{2(n+1)!} \frac{d^{n+1}}{dz^{n+1}} (G^{-1}(0)) \left(2 \int_0^t \|H(x)\| dx \right)^{n+1}. \quad (127)$$

This proves the induction step and hence the lemma. \square

C Circuit details for numerical implementations

In this section we discuss the circuit depth for the both Trotter and THRIFT algorithms, using arbitrary 2-qubit gates, for the transverse-field Ising model (1D and 2D cases), 1D Heisenberg model, and 1D Fermi-Hubbard model. We consider a Hamiltonian of the form $H = H_0 + \alpha H_1$, where H_0 is a sum of single-qubit terms (unless otherwise specified); $H_1 = \sum_{j=1}^K h_j$, with each h_j containing terms acting on disjoint qubits; and $\alpha \ll 1$. Exponentials of the terms in H_1 , $e^{-ih_j t}$, can therefore be implemented simultaneously with \mathcal{N}_j arbitrary 2-qubit gates. For all the models we consider, we have $\mathcal{N}_j = \mathcal{N}$, independent of j .

C.1 General facts about product formulas

C.1.1 Trotter formulas

The first-order Trotter approximation (Trotter 1) for the time-evolution operator $U = e^{-iHt}$ is

$$\mathcal{S}_1(t) = P_1^K(t), \quad (128)$$

with

$$P_a^b(z) = \left(\prod_{j=a}^{b-1} e^{-ih_j z} \right) e^{-iH_0 z} e^{-ih_b z}. \quad (129)$$

Since e^{-iH_0t} only requires single-qubit gates, Eq. (128) can be implemented with $K\mathcal{N}$ layers of arbitrary 2-qubit gates.

The second-order Trotter approximation (Trotter 2) can be written as

$$\mathcal{S}_2(t) = P_1^K(t/2)P_K^1(t/2) = P_1^{K-1}(t/2)e^{-ih_Kt}P_{K-1}^1(t/2), \quad (130)$$

and can be implemented with $(2K-1)\mathcal{N}$ layers of arbitrary 2-qubit gates. Note that if the number of Trotter layers is $N > 1$, one can merge the last exponential of the $(i-1)$ st step with the first of the (i) th step, giving a total arbitrary 2-qubit gate depth of $[(2K-2)N+1]\mathcal{N}$.

The fourth-order Trotter approximation (Trotter 4) can be obtained from Eq. (130) as [42]

$$\mathcal{S}_4(t) = \mathcal{S}_2(s_2t)^2\mathcal{S}_2((1-4s_2)t)\mathcal{S}_2(s_2t)^2, \quad \text{with } s_2 := (4 - \sqrt[3]{4})^{-1}. \quad (131)$$

The final term of each $\mathcal{S}_2(z)$ can be merged with the first term of the following $\mathcal{S}_2(z)$, so Eq. (131) can be implemented with $[5(2K-2)+1]\mathcal{N} = (10K-9)\mathcal{N}$ layers of arbitrary 2-qubit gates. As in the Trotter 2 case, if the number of Trotter layers is $N > 1$, one can merge the last time-evolution operator of the $(i-1)$ st step with the first of the (i) th step. This gives a total arbitrary 2-qubit gate depth of $[5(2K-2)N+1]\mathcal{N}$.

Finally, the optimised eighth-order Trotter approximation (optimised Trotter 8) is given by Eq. (15) in [23]

$$\mathcal{S}_8(t) = \left(\prod_{j=1}^m \mathcal{S}_2(\omega_{m-j+1}t) \right) \mathcal{S}_2(\omega_0t) \left(\prod_{j=1}^m \mathcal{S}_2(\omega_jt) \right), \quad (132)$$

with $m = 7$. Similarly to the previous case, one obtains that Eq. (132) can be implemented with $[15(2K-2)+1]\mathcal{N} = (30K-29)\mathcal{N}$ layers of arbitrary 2-qubit gates. If the number of Trotter layers is $N > 1$, one can merge the last time-evolution operator of the $(i-1)$ st step with the first of the (i) th step. This gives a total arbitrary 2-qubit gate depth of $[15(2K-2)N+1]\mathcal{N}$.

C.1.2 The ‘‘small A’’ formula of Omelyan et al.

In Ref. [18], Omelyan et al. derive an optimised fourth-order product formula for a Hamiltonian $H = H_0 + \alpha H_1$ with $\alpha \ll 1$. The error achieved by this formula scales as $O(\alpha^2t^5) + O(\alpha t^7)$. This implies that there exists a regime for small time t in which this formula achieves a scaling in α similar to THRIFT.

For a Hamiltonian $H = H_0 + \alpha H_1$, Omelyan et al.’s optimised formula can be written as [7, 18]

$$U_O(t) = e^{-ia_1H_0t}e^{-ib_1\alpha H_1t}e^{-ia_2H_0t}e^{-ib_2\alpha H_1t}e^{-ia_3H_0t}e^{-ib_2\alpha H_1t}e^{-ia_2H_0t}e^{-ib_1\alpha H_1t}e^{-ia_1H_0t}, \quad (133)$$

where the numerically determined coefficients are

$$\begin{aligned} a_1 &= 0.5316386245813512, \\ b_1 &= -0.04375142191737413, \\ a_2 &= -0.3086019704406066, \\ b_2 &= \frac{1}{2} - b_1, \\ a_3 &= 1 - 2 \sum_{i=1}^2 a_i. \end{aligned} \quad (134)$$

Since, for all the systems considered in this work, we have $H = \sum_{k=1}^{\Lambda} h_k$ with $\Lambda \geq 2$, we use the generalisation of Eq. (133) to Hamiltonians with an arbitrary number of terms given in Eq. (3) of Ref. [7]. In particular,

$$U_O(t) = \left(\prod_{k=1}^{\Lambda} e^{-ic_1h_kt} \right) \left(\prod_{k=\Lambda}^1 e^{-id_1h_kt} \right) \dots \left(\prod_{k=1}^{\Lambda} e^{-ic_4h_kt} \right) \left(\prod_{k=\Lambda}^1 e^{-id_4h_kt} \right), \quad (135)$$

where $c_i = a_i - d_{i-1}$ (with $d_0 = 0$) and $d_i = b_i - c_i$.

C.1.3 THRIFT formulas

The circuit depths for implementing a THRIFT approximation of order p are the same as the corresponding Trotter approximation applied to the original Hamiltonian with the rearrangement

$$H = \sum_{j=1}^K [(H_0 + h_j) - H_0] = \sum_{j=1}^K [h'_j - H_0], \quad (136)$$

where we assume that the exponential of each $h'_j := H_0 + h_j$ can be implemented with $\mathcal{N}'_j = \mathcal{N}'$ arbitrary 2-qubit gates. Note that particular care is required in cases where H_0 contains terms acting on more than one qubit, as in the 1D Fermi-Hubbard model case discussed in [Appendix C.2.4](#).

C.1.4 Magnus-THRIFT formulas

The first-order Magnus-THRIFT formula is given by [Eq. \(19\)](#) with $k = 1$,

$$\mathcal{S}_1^{\text{Magnus}}(t) = e^{-iH_0 t} e^{\Omega^{[1]}(t)}, \quad (137)$$

with

$$\Omega^{[1]}(t) = -i \int_0^t H_1(t_1) dt_1, \quad (138)$$

where $H_1(t) = e^{iH_0 t} H_1 e^{-H_0 t}$. In general, we can write $H_1(t) = \sum_{j=1}^P f_j(t) \tilde{h}_j$, where the exponential of each \tilde{h}_j can be implemented with $\tilde{\mathcal{N}}_j$ layers of arbitrary 2-qubit gates. Hence

$$\int_0^t H_1(t_1) dt_1 = \sum_{j=1}^P \left(\int_0^t f_j(t_1) dt_1 \right) \tilde{h}_j = \sum_{j=1}^P F_j(t) \tilde{h}_j = H_1^{\text{Magnus}}(t) \quad (139)$$

and

$$\mathcal{S}_1^{\text{Magnus}}(t) = e^{-iH_0 t} e^{-iH_1^{\text{Magnus}}(t)}. \quad (140)$$

Approximating the last term by a first-order Trotter formula, [Eq. \(140\)](#) can be implemented with $\sum_{j=1}^P \tilde{\mathcal{N}}_j$ layers of arbitrary 2-qubit gates.

The second-order Magnus-THRIFT formula is given by [Eq. \(19\)](#) with $k = 2$,

$$\mathcal{S}_2^{\text{Magnus}}(t) = e^{-iH_0 t} e^{\Omega^{[2]}(t)}, \quad (141)$$

with

$$\Omega^{[2]}(t) = -i \int_0^t H_1(t_1) dt_1 - \frac{1}{2} \int_0^t dt_1 \int_0^{t_1} dt_2 [H_1(t_1), H_1(t_2)]. \quad (142)$$

In this case, we can write $[H_1(t_1), H_1(t_2)] = \sum_{i,j=1}^P f_i(t_1) f_j(t_2) \tilde{h}_i \tilde{h}_j$, and therefore [Eq. \(142\)](#) becomes

$$\Omega^{[2]}(t) = -i \sum_{j=1}^{P'} g_j(t) \bar{h}_j, \quad (143)$$

with $P' \leq P^2$. The time-evolution operator of each term \bar{h}_j can be implemented with arbitrary 2-qubit gate depth $\tilde{\mathcal{N}}_j$. Approximating $e^{\Omega^{[2]}(t)}$ by a second-order Trotter formula and assuming for simplicity that $\tilde{\mathcal{N}}_j = \tilde{\mathcal{N}}$ for all j , we find that a single Trotter layer of [Eq. \(141\)](#) can be implemented with arbitrary 2-qubit gate depth $(2P' - 1)\tilde{\mathcal{N}}$ and $N > 1$ Trotter layers with arbitrary 2-qubit gate depth $[(2P' - 2)N + 1]\tilde{\mathcal{N}}$. Note that, in general, the terms \bar{h}_j may contain multi-qubit terms and therefore $\tilde{\mathcal{N}}$ depends on the specific model. In the next section we discuss the case of the 1D transverse-field Ising model.

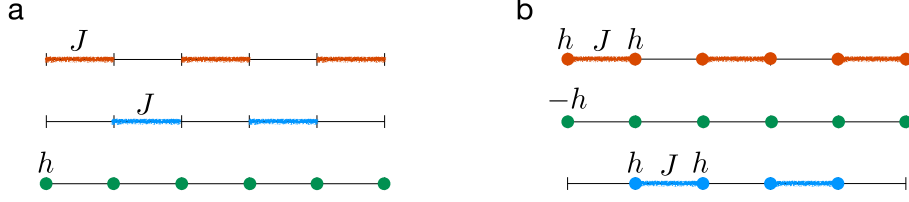


Figure 7: Partitions for implementing the first-order (a) Trotter and (b) THRIFT formulas in the 1D TFIM and 1D Heisenberg models. (a) One layer of the first-order Trotter approximation for these models is obtained by approximating e^{-iHt} as $e^{-ih_1^{\text{odd}}t} e^{-ih_1^{\text{even}}t} e^{-iH_0t}$. (b) One layer of the first-order THRIFT approximation is obtained by approximating e^{-iHt} as $e^{-i(h_1^{\text{odd}}+H_0)t} e^{iH_0t} e^{-i(h_1^{\text{even}}+H_0)t} e^{-iH_0t}$. Here, $h_1^{\text{even/odd}} = h_{XX}^{\text{even/odd}}$ for the 1D transverse-field Ising model and $h_1^{\text{even/odd}} = h_{XX+YY+ZZ}^{\text{even/odd}}$ for the 1D Heisenberg model. In each row of both panels, all the single-qubit (dots) and 2-qubit (thick lines) terms are implemented simultaneously.

C.2 Applications to specific models

C.2.1 1D transverse-field Ising model

For the 1D transverse-field Ising model, we have $H_{\text{TFIM}} = H_0 + JH_1$ with H_0 acting on single qubits only and $H_1 = h_{XX}^{\text{even}} + h_{XX}^{\text{odd}}$ (hence $K = P = 2$), with $h_{XX}^{\text{even/odd}} = \sum_j X_j X_{j+1}$. The time-evolution operators associated with such terms can be implemented with $\mathcal{N} = 1$ layer of arbitrary 2-qubit gates (or two layers of CNOT gates) each. Since the cost to implement the time-evolution operator of $h_{XX}^{\text{even/odd}} + H_0$ is the same as $h_{XX}^{\text{even/odd}}$ in terms of both arbitrary 2-qubit gates and CNOT gates, the circuit depth for a p th-order THRIFT formula is the same as for the corresponding Trotter formula.

For Omelyan et al.'s optimised small A formula, we have $\Lambda = 3$, and we identify $h_1 = H_0$, $h_2 = \alpha h_{XX}^{\text{even}}$, and $h_3 = \alpha h_{XX}^{\text{odd}}$. Recalling that H_0 can be implemented via single-qubit gates and merging the last exponential inside a bracket in Eq. (135) with the first exponential of the following one, we find that the arbitrary 2-qubit gate cost to implement N layers of Eq. (135) is $12N$ (corresponding to $24N$ layers of CNOT gates).

For Magnus-THRIFT 1 we have

$$H_1(t) = f_{XX}(t)H_{XX} + f_{YY}(t)H_{YY} + f_{XY+YX}(t)H_{XY+YX}, \quad (144)$$

with $H_{XX} = \sum_j X_j X_{j+1}$, $H_{YY} = \sum_j Y_j Y_{j+1}$, $H_{XY+YX} = \sum_j (X_j Y_{j+1} + Y_j X_{j+1})$, and $f_i(t)$ time-dependent coefficients. Similarly to the previous cases, $H_1(t)$ can be split into even/odd contributions, each of which can be implemented with one layer of arbitrary 2-qubit gates (or two CNOT gates). Hence, we have $P = 2$ and $\tilde{\mathcal{N}}_j = \tilde{\mathcal{N}} = 1$: $N > 1$ layers of the Magnus-THRIFT 1 formula in Eq. (140) can be implemented with $2N$ layers of arbitrary 2-qubit gates (or $4N$ layers of CNOT gates). For Magnus-THRIFT 2, Eq. (142) can be written as

$$\begin{aligned} \Omega^{[2]}(t) &\propto f_{XX}(t)H_{XX} + f_{YY}(t)H_{YY} + f_{XY+YX}(t)H_{XY+YX} \\ &\quad + f_{XZY+YZX}(t)H_{XZY+YZX} + f_{XZX}(t)H_{XZX} + f_{YZY}(t)H_{YZY} \\ &\quad + \text{single-qubit terms.} \end{aligned} \quad (145)$$

Here, $H_{XZY+YZX} = \sum_j X_j Z_{j+1} Y_{j+2} + Y_j Z_{j+1} X_{j+2}$, $H_{XZX} = \sum_j X_j Z_{j+1} X_{j+2}$, $H_{YZY} = \sum_j Y_j Z_{j+1} Y_{j+2}$, and the various $f_i(t)$ denote the corresponding time-dependent coefficients. Since the terms in the second line of Eq. (145) act on three qubits, $\Omega^{[2]}(t)$ has to be split into three groups as shown in Fig. 8(a). Moreover, one can show numerically that the time-evolution operator of each group can be implemented with 3 layers of arbitrary 2-qubit gates (corresponding to 9 layers of CNOT gates). Hence, the second-order Magnus-THRIFT formula for the 1D transverse-field Ising model one has $P' = 3$ and $\tilde{\mathcal{N}}_j = \tilde{\mathcal{N}} = 3$, corresponding to an arbitrary 2-qubit gate depth of $12N + 3$ (and CNOT gate depth of $36N + 9$).

C.2.2 2D transverse-field Ising model

For the 2D transverse-field Ising model we have $H_{\text{TFIM}} = H_0 + JH_1$, with $H_1 = H_{XX}^h + H_{XX}^v = h_{XX}^{\text{h,even}} + h_{XX}^{\text{h,odd}} + h_{XX}^{\text{v,even}} + h_{XX}^{\text{v,odd}}$, with the h and v superscripts denoting horizontal and vertical terms, respectively. Hence, we have

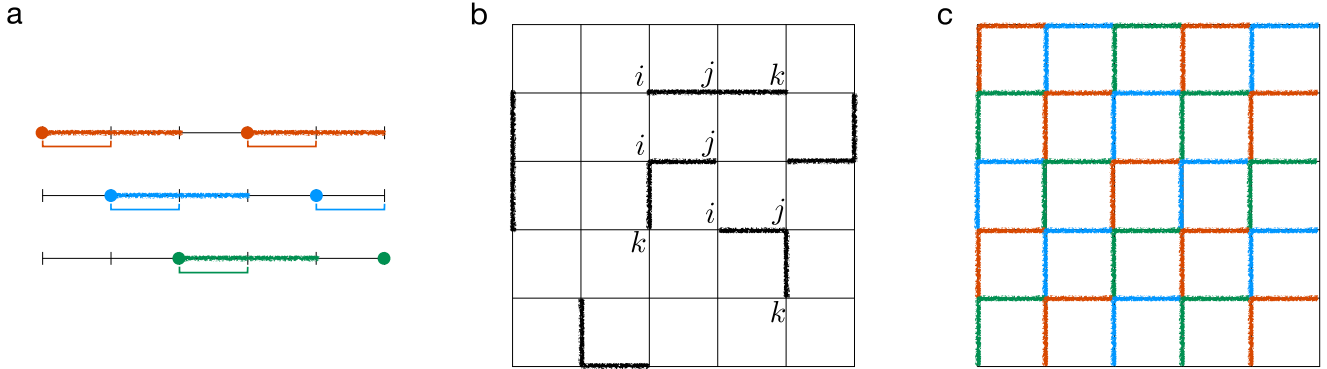


Figure 8: Partitions for implementing the second-order Magnus-THRIFT formula in the 1D (a) and 2D (b,c) transverse-field Ising model. (a) One of the possible groupings of the terms in $\Omega^{[2]}(t)$ in Eq. (145). In each one of the three subgroups, all the single-qubit (dots), 2-qubit (thin lines), and three-qubit (thick lines) terms are implemented simultaneously. (b) In the 2D transverse-field Ising model, there are six possible configurations for each of the three-qubit terms in $\Omega^{[2]}(t)$ in Eq. (145). (c) In order to implement $e^{\Omega^{[2]}(t)}$, each of the six possible configurations can be split into three layers of terms that can be implemented simultaneously.

$K = 4$. The time-evolution operator corresponding to each term can be implemented with a layer of $\mathcal{N} = 1$ arbitrary 2-qubit gates (or 2 CNOT gates). Similarly to the 1D case, one can implement the time-evolution operators of $h_{XX}^{\text{h/v,even/odd}} + H_0$ occurring in THRIFT formulas with the same cost.

For Omelyan et al.'s optimised small A formula we have $\Lambda = 5$, with $h_1 = H_0$, $h_2 = \alpha h_{XX}^{\text{h,even}}$, $h_3 = \alpha h_{XX}^{\text{h,odd}}$, $h_4 = \alpha h_{XX}^{\text{v,even}}$, and $h_5 = \alpha h_{XX}^{\text{v,odd}}$ (see Appendix C.2.2). With similar arguments as in the 1D case, we find that the arbitrary 2-qubit gate cost to implement N layers of Eq. (135) is $28N$ (or $56N$ layers of CNOT gates).

In Magnus-THRIFT 1, $H_1(t)$ has the same form as Eq. (144) and can be split into four terms as the original H_1 . Therefore, we find $P = 4$ and $\tilde{\mathcal{N}}_j = \tilde{\mathcal{N}} = 1$: $N > 1$ layers of the Magnus-THRIFT 1 formula in Eq. (140) can be implemented with $4N$ layers of arbitrary 2-qubit gates (or $8N$ layers of CNOT gates).

The implementation of the second-order Magnus-THRIFT approximation requires more care. The functional form of $\Omega^{[2]}(t)$ is the same as in Eq. (145), but each of the three-qubit Hamiltonians $H_{XZY+YZX}$, H_{XZX} , and H_{YZY} has now a 2D nature. For instance, $H_{XZX} = \sum_{\langle i,j \rangle} \sum_{k \in \text{neigh}(\{i,j\})} X_i Z_j X_k$: here, i, j are nearest-neighbors and k is a nearest-neighbor of either i or j . Hence, for a given choice of i, j , there are 2 linear (vertical and horizontal) and 4 two-dimensional “L”-shaped independent configurations (see Fig. 8(b)). The time-evolution operators corresponding to each of these terms can be implemented in 3 layers as shown in Fig. 8(c). Then, $P' = 18$. In turn, we numerically verified that each layer can be implemented with $\tilde{\mathcal{N}} = 3$ arbitrary-two qubit gates (or 9 CNOT gates). The overall arbitrary 2-qubit (CNOT) gate depth to implement $N > 1$ steps is therefore $102N + 3$ ($306N + 9$).

C.2.3 1D Heisenberg model

Similarly to the 1D transverse-field Ising model, for the 1D Heisenberg model we have $H_{\text{Heisenberg}} = H_0 + JH_1$ with H_0 acting on single qubits only and $H_1 = H_{XX} + H_{YY} + H_{ZZ} = h_{XX+YY+ZZ}^{\text{even}} + h_{XX+YY+ZZ}^{\text{odd}}$ (hence $K = 2$), with $h_{XX+YY+ZZ}^{\text{even/odd}} = \sum_j \text{even/odd} (X_j X_{j+1} + Y_j Y_{j+1} + Z_j Z_{j+1})$. Therefore, the circuit depths for Trotter and THRIFT formulas for the 1D Heisenberg model can be obtained by following the same steps as the 1D transverse-field Ising model discussed in Appendix C.2.1. The same holds for Omelyan et al.'s optimised small A formula, where $\Lambda = 3$ and we identify $h_1 = H_0$, $h_2 = \alpha h_{XX+YY+ZZ}^{\text{even}}$, and $h_3 = \alpha h_{XX+YY+ZZ}^{\text{odd}}$. In particular, the arbitrary 2-qubit gate depths for the various formulas are the same, while to obtain the CNOT gate depths, one has to take into account that the time-evolution operator associated with $h_{XX+YY+ZZ}^{\text{even/odd}}$ uses 3 layers of CNOT gates.

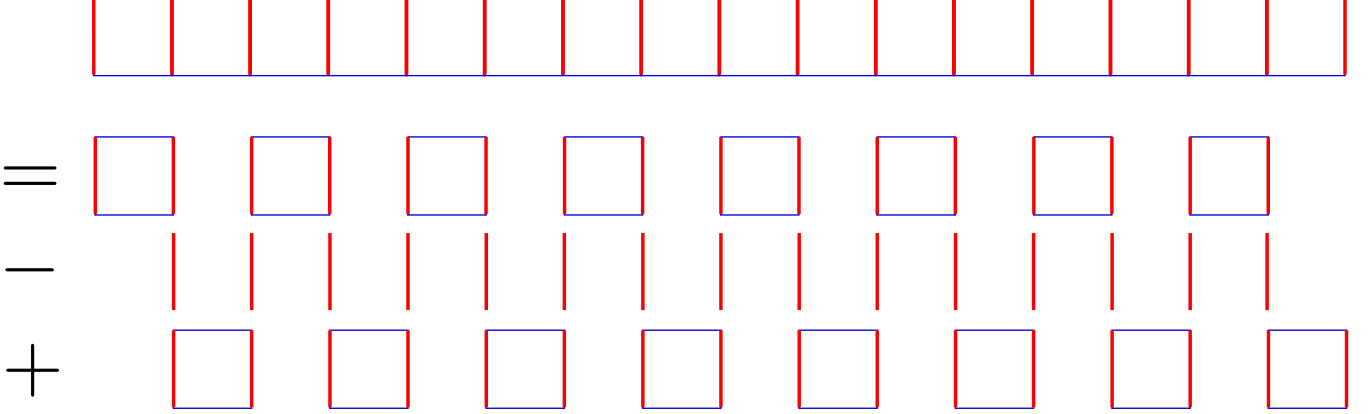


Figure 9: Partition of terms for THRIFT in the 1D Fermi-Hubbard model. Vertical lines (red) correspond to the on-site interaction, while horizontal lines (blue) correspond to the hopping terms. Taking $H_0 = \sum_j n_{j\uparrow} n_{j\downarrow}$ leads to a partition where 4 qubit gates are needed.

C.2.4 1D Fermi-Hubbard model

The Hamiltonian of the Fermi-Hubbard model can be written as $H_{\text{FH}} = H_0 + t_{\text{hop}} H_1$, with $H_0 = H_{\text{int}}$ and $H_1 = H_{\text{hop}} = h_{\text{hop}}^{\text{even}} + h_{\text{hop}}^{\text{odd}}$, with $h_{\text{hop}}^{\text{even/odd}} = -\sum_{\sigma} \sum_i \text{even/odd} (c_{i,\sigma}^{\dagger} c_{i+1,\sigma} + c_{i+1,\sigma}^{\dagger} c_{i,\sigma})$. The time-evolution operator corresponding to each term of this decomposition can be implemented with one layer of arbitrary 2-qubit gates (and 2 layers of CNOT gates). Hence, we find $K = 3$ and $\mathcal{N} = 1$.

For Omelyan et al.'s optimised small A formula we have $\Lambda = 3$ with $h_1 = H_{\text{int}}$, $h_2 = \alpha h_{\text{hop}}^{\text{even}}$, and $h_3 = \alpha h_{\text{hop}}^{\text{odd}}$ (see Appendix C.2.4). In contrast to the previous cases, here H_0 can be implemented with one layer of arbitrary 2-qubit gates. Hence, the overall arbitrary 2-qubit gate cost to implement N layers of Eq. (135) is $16N + 1$ (corresponding to $32N + 2$ layers of CNOT gates). Note that, to obtain this number, one needs to merge the last term $e^{-id_4 H_{\text{int}} t}$ of the i th Trotter layer with the first term $e^{-ic_1 H_{\text{int}} t}$ of the $(i + 1)$ st layer.

Finally, there are some additional considerations to obtain the 2-qubit gate depth for THRIFT formulas. In this case, H_0 is not a single-qubit Hamiltonian and implementing $e^{\pm i H_0 t}$ requires $\mathcal{N}'_0 = 1$ layer of arbitrary 2-qubit gates (corresponding to 2 layers of CNOT gates). As shown in Fig. 9, each of the $K = 2$ THRIFT partitions $[H_0 + H^{\text{even/odd}}]$ consist of terms acting on four qubits and implementing $e^{-i(H_0 + H^{\text{even/odd}})t}$ requires 3 layers of arbitrary 2-qubit gates (and 6 layers of CNOT gates). Hence, $\mathcal{N}'_1 = 3$. The overall arbitrary 2-qubit (CNOT) gate depth can be computed by taking into account both these facts. For instance, $N > 1$ layers of the second-order THRIFT formula can be implemented with arbitrary 2-qubit gate depth $[(2K - 2)\mathcal{N}'_1 + 2\mathcal{N}'_0]N + \mathcal{N}'_1 = 8N + 3$.

D Additional numerical results

In Section 4 we showed the 2-qubit gate depth d to achieve a fixed precision ϵ for different system sizes L at evolution time $T = L$. In this section we provide a more detailed analysis by showing the results at different values of the small parameter α , performing weighted linear regression to the power laws describing the depth d as a function of L , and comparing the power laws thus obtained to the theoretically expected results.

For later reference we note that for ordinary k th-order Trotter methods, the depth to achieve error ϵ scales for evolution time T in a system of size L scales as

$$d_{\text{trotter},k} = O\left(\epsilon^{-\frac{1}{k}} \alpha^{\frac{1}{k}} L^{\frac{1}{k}} T^{1+\frac{1}{k}}\right) \quad (146)$$

if we choose a splitting of the Hamiltonian that has H_0 as one term and all other terms scale linear with α . For a k th-order THRIFT formula, almost the same is true; the only difference is that the commutator bounds now give a factor of α^2 , so the depth scales as

$$d_{\text{thrift},k} = O\left(\epsilon^{-\frac{1}{k}} \alpha^{\frac{2}{k}} L^{\frac{1}{k}} T^{1+\frac{1}{k}}\right). \quad (147)$$

These two expressions follow simply from combining the ordinary Trotter error bounds, or THRIFT error bounds given in [Theorem 1](#), with the analysis from [Appendix A.1](#). Because we only consider geometrically local Hamiltonians, [Eqs. \(146\) and \(147\)](#) hold with ϵ denoting the worst-case error, as in [Fig. 2](#), as well as when ϵ is the average case error, as in [Figs. 4 and 6](#), by the same analysis done for [Theorem 2](#) in [\[35\]](#).

D.1 Transverse-field Ising model

In [Fig. 10](#) we analyse in more detail the 2-qubit depth required to achieve a worst-case error $\|U - U_{\text{exact}}\| < 0.01$ for the different TDS methods as a function of system size L and evolution time T (1D case) or only evolution time T (2D case). On the left we show the 2-qubit gate depth d at fixed $\alpha = 1/8$ and see that it is well described by a power law of the form $d = aL^k$ (1D) or $d = aT^k$ (2D). On the right we plot the prefactor a and exponent k as a function of α . In the 1D case, the exponents of the second- and fourth-order methods match the theoretically expected values of 2 and 1.5 very well. The same is true for the optimised eighth-order formula where the exponent is ≈ 1.125 for all α . The exponents of the first- and second-order methods match. This is because the transverse-field Ising model Hamiltonian and $H_1(t)$ both can be decomposed into only two terms that are exactly implementable, in which case the first-order Trotter formula has the same scaling as the second-order formula. The fit exponent of the optimised THRIFT 8 formula, on the other hand, does not match the theoretically expected value and is below 1 for all α , despite the very accurate fits shown on the left. Instead we find that a scales roughly as $\alpha^{\frac{2}{k}}$ for second-, fourth-, and eighth-order THRIFT *and* Trotter methods, although the prefactors a of the THRIFT methods are always below those of the corresponding Trotter method. Again, the first-order methods behave similarly to the second-order methods and a is roughly linear in a for both Magnus-THRIFT methods.

In the 2D case the fit exponents do not fall as nicely into distinct groups, but we observe again that, with the notable exception of Trotter 1, all first- and second-order methods have exponent $k \approx 1.5$ as theoretically expected for second-order methods. The fourth-order methods have $k \approx 1.25$, again in line with theoretical expectations. Trotter 1 and the optimised THRIFT 8 formula, on the other hand, deviate substantially from the theoretical expectation with $k \approx 1$ and $k \approx 0.5$, respectively. This suggests that the optimised THRIFT 8 formula can be used to fast forward the transverse-field Ising model. While the 1D transverse-field Ising model is integrable, this is more surprising in the 2D case and may be an artifact of the fairly small system size considered here. For the prefactors a , we find the same as in 1D: they have d scaling like $\alpha^{\frac{2}{k}}$ for THRIFT *and* Trotter methods, i.e., as theoretically expected for the THRIFT methods.

D.2 1D Heisenberg model

In [Fig. 11](#) we analyse the 2-qubit gate depth to achieve an average infidelity $\mathbb{E}_{\{|x\rangle\}}[1 - |\langle x|U_{\text{exact}}^\dagger U|x\rangle|^2] \leq 0.01$ as a function of the system size L , evolution time T , and interaction strength $J = \alpha$. On the left we show the 2-qubit gate depth at fixed $\alpha = \frac{1}{8}$, which is well described by a power law of the form $d = aL^k$. We find that this remains true for different choices of α , where the coefficients a and k depend on α . On the right we show the coefficients obtained via weighted linear regression as a function of α . While the situation is not as clear cut as for the transverse-field Ising model in [Fig. 10](#), the algorithms (with maybe the exception of the optimised small A method) still appear to fall into two groups: the first- and second-order methods, for which (at least for larger $\alpha \gtrsim 0.2$) $k \approx 1.75$, and the higher-order methods, for which (again, at least for $\alpha \gtrsim 0.2$) $k \approx 1.25$.

D.3 1D Fermi-Hubbard model

The same analysis done for the transverse-field Ising model and Heisenberg model in [Figs. 10 and 11](#) is repeated for the Fermi-Hubbard model in [Fig. 12](#). Again, we use the average infidelity $\mathbb{E}_{\{|x\rangle\}}[1 - |\langle x|U_{\text{exact}}^\dagger U|x\rangle|^2] \leq 0.01$ as a figure of merit to be able to reach larger system sizes in our simulations. Again, we find robust power laws for the 2-qubit depth to get the average infidelity below threshold as we increase the system size L and scale the evolution time as $T = L$, as exemplified for $\alpha = 1/16$ in the left of [Fig. 12](#). On the right we plot the exponents k and prefactors a of that power law as a function of α .

As in the case of Heisenberg model ([Fig. 11](#)), the algorithms do not fall as neatly into groups with different exponents as for the transverse-field Ising model ([Fig. 10](#)). Trotter 1 and 2 have $k \approx 1.75$ for all α , and Trotter 4 and the optimised Trotter 8 formula have $1 \lesssim k \lesssim 1.25$ for all α , but also fairly large uncertainties. For THRIFT 1

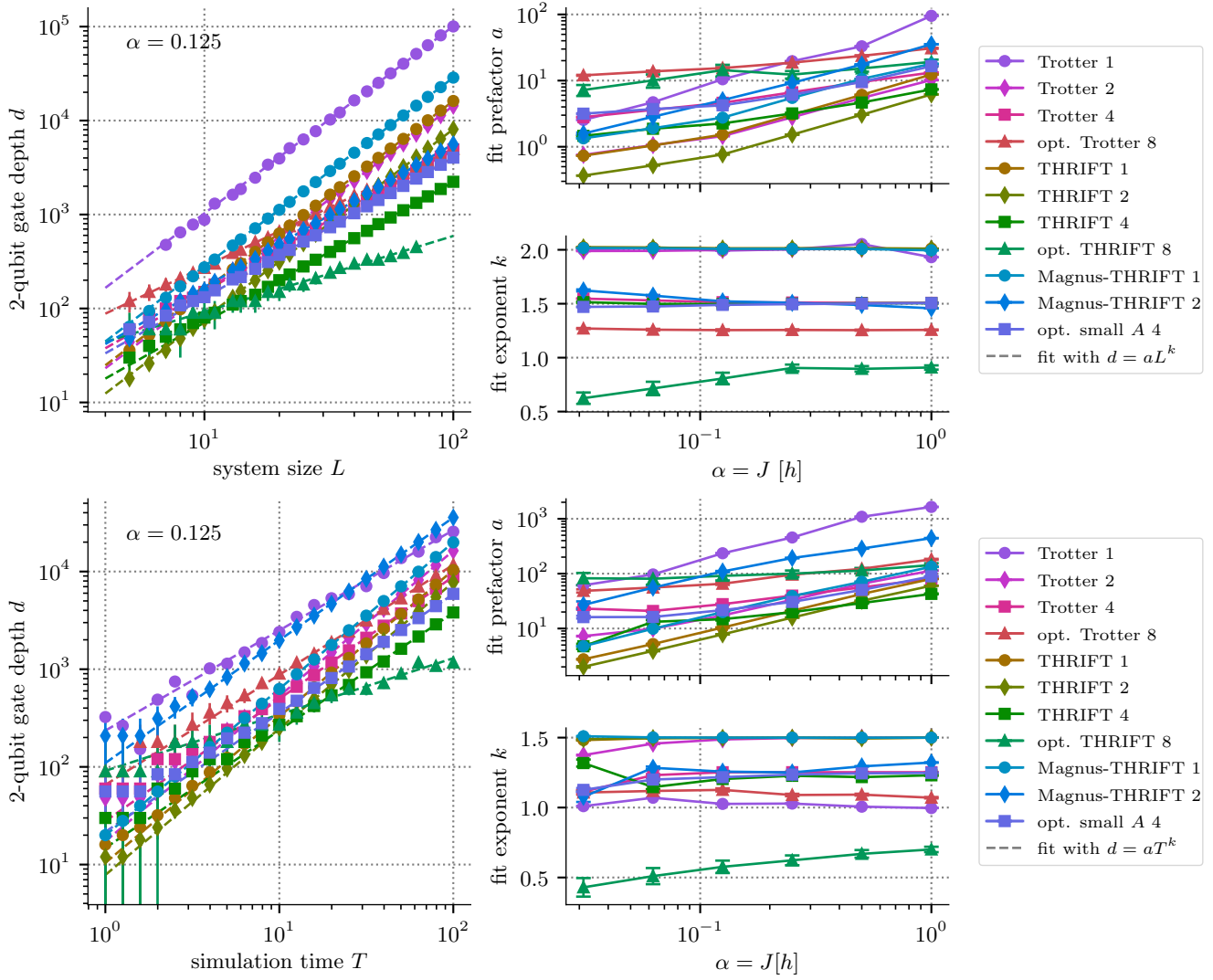


Figure 10: Performance scaling for the 1D (top) and 2D (bottom) transverse field Ising model. (left) The same data as in Fig. 2 to provide context to the fit parameters shown on the right. (right) Fit parameters of a power law $d = aL^k$ or $d = aT^k$, respectively, to the data shown on the left for different values of α , obtained via weighted linear regression.

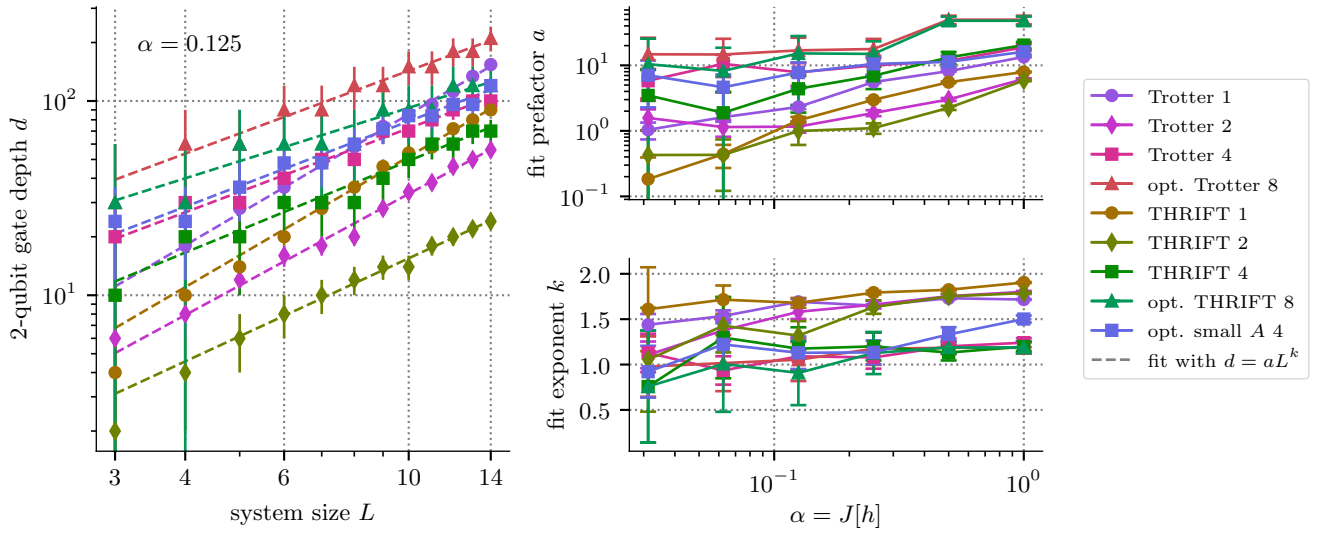


Figure 11: Performance scaling for the 1D Heisenberg chain. (left) The same data as in Fig. 4 to provide context for the fit parameters shown on the right. (right) Fit parameters for the data shown on the left for different values of α , obtained via weighted linear regression.

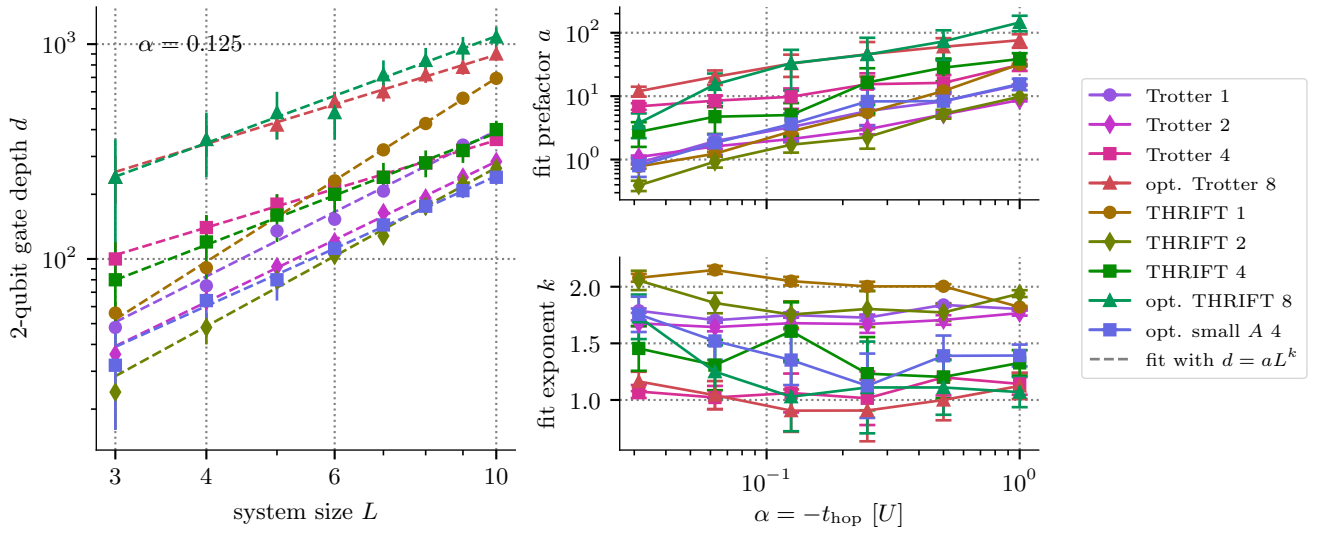


Figure 12: Performance scaling for the 1D Fermi-Hubbard model. (left) The same data as in Fig. 6 to provide context for the fit parameters shown on the right. (right) Fit parameters to the data shown on the left for different values of α . The error bars are the fit uncertainties when taking the error bars from the left as the uncertainties of the original data.

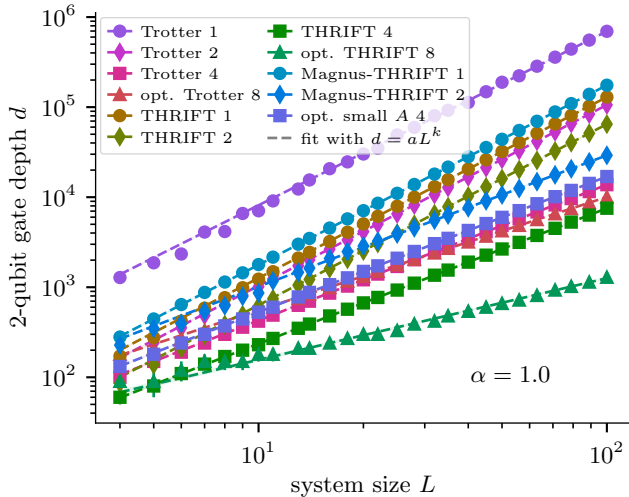


Figure 13: 2-qubit gate depth to achieve $\|U - U_{\text{exact}}\| \leq 0.01$ for the different TDS algorithms for a field strength of $J = 1$ and evolution time $T = L$, for a $1 \times L$ Ising chain with transverse field $h = 1$. In contrast to Fig. 2, we have $\alpha = 1$, so Theorem 1 does not predict that THRIFT methods should outperform Trotter methods. Nevertheless, THRIFT uses shallower circuits to achieve the desired precision than the corresponding Trotter methods.

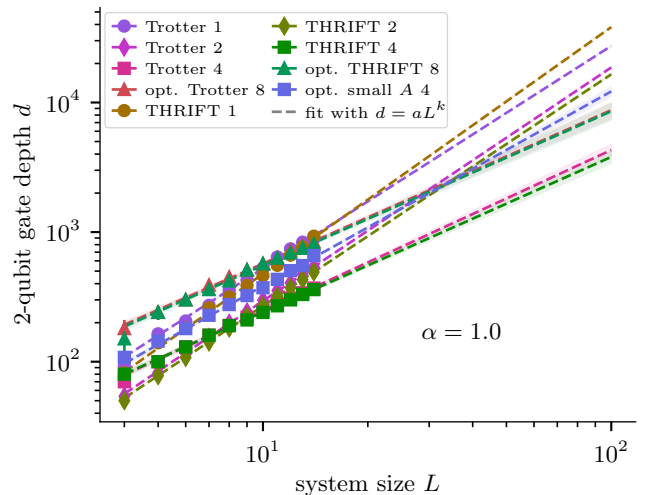


Figure 14: 2-qubit depth to achieve average infidelity $\mathbb{E}_{\{|x\rangle\}}[1 - |\langle x|U_{\text{exact}}^\dagger U|x\rangle|^2] \leq 0.01$ for the different TDS algorithms for a $1 \times L$ Heisenberg chain with field strength of $J = 1$ and evolution time $T = L$. In contrast to Fig. 4, we have $\alpha = 1$ here, so Theorem 1 does not predict that THRIFT methods should outperform Trotter methods. Nevertheless, THRIFT uses almost the same circuit depth as the corresponding Trotter methods to achieve the target precision.

and 2, k varies between 2.25 and 1.75, and for THRIFT 4 and 8, it decreases with α from $k \approx 1.75$ at $\alpha = 1/32$ to $k \approx 1.25$ at $\alpha = 1$.

D.4 TFIM and Heisenberg model with strong interactions $\alpha = 1$

Figures 1 and 3 indicate that the THRIFT methods perform well for the transverse-field Ising model and Heisenberg model not only in the theoretically expected $\alpha \ll 1$ limit, but also for $\alpha \sim 1$. In Figs. 13 and 14 we show that this is indeed the case by repeating the numerics done for $\alpha = 1/8$ in Figs. 2 and 4, now taking the larger value $\alpha = 1$. We find that for the transverse-field Ising model, the THRIFT circuits use lower depth than Trotter circuits to achieve a desired precision even at $J = h$, and that for the Heisenberg model, the depths are very similar for the THRIFT and Trotter methods.

References

- [1] D. W. Berry, G. Ahokas, R. Cleve and B. C. Sanders, “Efficient quantum algorithms for simulating sparse Hamiltonians”, *Commun. Math. Phys.* **270**, 359–371 (2006).
- [2] A. M. Childs and R. Kothari, “Limitations on the simulation of non-sparse Hamiltonians”, *Quantum Inf. Comput.* **10**, 669–684 (2010).
- [3] A. M. Childs, “On the relationship between continuous- and discrete-time quantum walk”, *Commun. Math. Phys.* **294**, 581–603 (2009).
- [4] A. M. Childs and N. Wiebe, “Hamiltonian simulation using linear combinations of unitary operations”, *Quantum Inf. Comput.* **12**, 901–924 (2012).
- [5] D. W. Berry, A. M. Childs, R. Cleve, R. Kothari and R. D. Somma, “Exponential improvement in precision for simulating sparse Hamiltonians”, in *Proceedings of the forty-sixth annual ACM symposium on theory of computing* (2014).
- [6] G. H. Low and I. L. Chuang, “Optimal Hamiltonian simulation by quantum signal processing”, *Phys. Rev. Lett.* **118**, 010501 (2017).
- [7] J. Ostmeier, “Optimised Trotter decompositions for classical and quantum computing”, *J. Phys. A* **56**, 285303 (2023).
- [8] C. Mc Keever and M. Lubasch, “Classically optimized Hamiltonian simulation”, *Phys. Rev. Res.* **5**, 023146 (2023).
- [9] M. S. J. Tepaske, D. Hahn and D. J. Luitz, “Optimal compression of quantum many-body time evolution operators into brickwall circuits”, *SciPost Phys.* **14**, 073 (2023).
- [10] A. M. Childs, D. Maslov, Y. Nam, N. J. Ross and Y. Su, “Toward the first quantum simulation with quantum speedup”, *Proc. Natl. Acad. Sci. U.S.A.* **115**, 9456–9461 (2018).
- [11] A. M. Childs and Y. Su, “Nearly optimal lattice simulation by product formulas”, *Phys. Rev. Lett.* **123**, 050503 (2019).
- [12] A. M. Childs, Y. Su, M. C. Tran, N. Wiebe and S. Zhu, “Theory of Trotter error with commutator scaling”, *Phys. Rev. X* **11**, 011020 (2021).
- [13] G. H. Low and N. Wiebe, *Hamiltonian simulation in the interaction picture*, 2019, [arXiv:1805.00675](https://arxiv.org/abs/1805.00675).
- [14] E. Manousakis, “The spin- $\frac{1}{2}$ Heisenberg antiferromagnet on a square lattice and its application to the cuprous oxides”, *Rev. Mod. Phys.* **63**, 1–62 (1991).
- [15] P. Fazekas, *Lecture notes on electron correlation and magnetism*, Series in Modern Condensed Mat (World Scientific, 1999).
- [16] Y. Zhou, K. Kanoda and T.-K. Ng, “Quantum spin liquid states”, *Rev. Mod. Phys.* **89**, 025003 (2017).
- [17] J. Haah, M. B. Hastings, R. Kothari and G. H. Low, “Quantum algorithm for simulating real time evolution of lattice Hamiltonians”, *SIAM J. Comput.*, 250–284 (2021).
- [18] I. Omelyan, I. Mryglod and R. Folk, “Optimized Forest–Ruth- and Suzuki-like algorithms for integration of motion in many-body systems”, *Comput. Phys. Commun.* **146**, 188–202 (2002).
- [19] A. Fetter and J. Walecka, *Quantum theory of many-particle systems*, Dover Books on Physics (Dover Publications, 2003).
- [20] J. Huyghebaert and H. D. Raedt, “Product formula methods for time-dependent Schrödinger problems”, *J. Phys. A* **23**, 5777 (1990).
- [21] D. Poulin, A. Qarry, R. Somma and F. Verstraete, “Quantum simulation of time-dependent Hamiltonians and the convenient illusion of Hilbert space”, *Phys. Rev. Lett.* **106**, 170501 (2011).
- [22] M. Suzuki, “General theory of fractal path integrals with applications to many-body theories and statistical physics”, *J. Math. Phys.* **32**, 400–407 (1991).
- [23] M. E. S. Morales, P. C. S. Costa, D. K. Burgarth, Y. R. Sanders and D. W. Berry, *Greatly improved higher-order product formulae for quantum simulation*, 2022, [arXiv:2210.15817](https://arxiv.org/abs/2210.15817).

- [24] W. Magnus, “On the exponential solution of differential equations for a linear operator”, *Commun. Pure Appl. Math.* **7**, 649–673 (1954).
- [25] F. Fer, “Résolution de l’équation matricielle $du/dt = pu$ par produit infini d’exponentielles matricielles”, *Bull. Cl. Sci., Acad. R. Belg.* **44**, 818–829 (1958).
- [26] S. Blanes, F. Casas, J. Oteo and J. Ros, “The Magnus expansion and some of its applications”, *Phys. Rep.* **470**, 151–238 (2009).
- [27] S. Klarsfeld and J. A. Oteo, “Recursive generation of higher-order terms in the Magnus expansion”, *Phys. Rev. A* **39**, 3270–3273 (1989).
- [28] S. Blanes, F. Casas, J. A. Oteo and J. Ros, “Magnus and fer expansions for matrix differential equations: the convergence problem”, *J. Phys. A* **31**, 259 (1998).
- [29] P. C. Moan, *Efficient approximation of Sturm-Liouville problems using Lie-group methods*, Numerical Analysis Reports (University of Cambridge, Department of Applied Mathematics and Theoretical Physics, 1998).
- [30] A. Iserles, “Solving linear ordinary differential equations by exponentials of iterated commutators”, *Numer. Math.* **45**, 183–199 (1984).
- [31] H. Yoshida, “Construction of higher order symplectic integrators”, *Phys. Lett. A* **150**, 262–268 (1990).
- [32] B. M. Terhal and D. P. DiVincenzo, “Classical simulation of noninteracting-fermion quantum circuits”, *Phys. Rev. A* **65**, 032325 (2002).
- [33] S. Bravyi and R. König, “Disorder-assisted error correction in Majorana chains”, *Commun. Math. Phys.* **316**, 641–692 (2012).
- [34] J. L. Bosse, *FLOYao.jl – a fermionic linear optics simulator backend for Yao.jl*, 2022.
- [35] Q. Zhao, Y. Zhou, A. F. Shaw, T. Li and A. M. Childs, “Hamiltonian simulation with random inputs”, *Phys. Rev. Lett.* **129**, 270502 (2022).
- [36] C. Cade, L. Mineh, A. Montanaro and S. Stanisic, “Strategies for solving the Fermi-Hubbard model on near-term quantum computers”, *Phys. Rev. B* **102**, 235122 (2020).
- [37] M. Heyl, “Dynamical quantum phase transitions: a review”, *Rep. Prog. Phys.* **81**, 054001 (2018).
- [38] Etienne (<https://math.stackexchange.com/users/80469/etienne>), *Assume that $f \in L([a, b])$ and $\int x^n f(x)dx = 0$ for $n = 0, 1, 2, \dots$* . Mathematics Stack Exchange, URL:<https://math.stackexchange.com/q/876642> (version: 2014-07-24), eprint: <https://math.stackexchange.com/q/876642>.
- [39] E. T. Bell, “Exponential polynomials”, *Ann. Math.* **35**, 258–277 (1934).
- [40] L. Comtet, *Advanced combinatorics: the art of finite and infinite expansions* (Springer Netherlands, 1974).
- [41] A. D. D. Craik, “Prehistory of Faà di Bruno’s formula”, *Am. Math. Mon.* **112**, 119–130 (2005).
- [42] N. Hatano and M. Suzuki, “Finding exponential product formulas of higher orders”, in *Quantum annealing and other optimization methods* (Springer Berlin, Heidelberg, 2005), pp. 37–68.